Journal of Pharmacokinetics and Pharmacodynamics
https://doi.org/10.1007/s10928-017-9560-y

ORIGINAL PAPER

Transit and lifespan in neutrophil production: implications for drug intervention

Daniel Câmara De Souza[1] · Morgan Craig[2] · Tyler Cassidy[1] · Jun Li[3] · Fahima Nekka[3] · Jacques Bélair[4] · Antony R. Humphries[5]

Received: 22 May 2017 / Accepted: 6 December 2017

Abstract

A comparison of the transit compartment ordinary differential equation modelling approach to distributed and discrete delay differential equation models is studied by focusing on Quartino's extension to the Friberg transit compartment model of myelosuppression, widely relied upon in the pharmaceutical sciences to predict the neutrophil response after chemotherapy, and on a QSP delay differential equation model of granulopoiesis. An extension to the Quartino model is provided by considering a general number of transit compartments and introducing an extra parameter that allows for the decoupling of the maturation time from the production rate of cells. An overview of the well established linear chain technique, used to reformulate transit compartment models with constant transit rates as distributed delay differential equations (DDEs), is then given. A state-dependent time rescaling of the Quartino model is performed to apply the linear chain technique and rewrite the Quartino model as a distributed DDE, yielding a discrete DDE model in a certain parameter limit. Next, stability and bifurcation analyses are undertaken in an effort to situate such studies in a mathematical pharmacology context. We show that both the original Friberg and the Quartino extension models incorrectly define the mean maturation time, essentially treating the proliferative pool as an additional maturation compartment. This mis-specification can have far reaching consequences on the development of future models of myelosuppression in PK/PD.

Keywords Granulopoiesis · Mathematical pharmacology · Delay differential equations · Bifurcation analyses · Transit compartment models · Linear chain technique

Introduction

In the pharmaceutical sciences, the concept of lag time, or the delay between the administration and the absorption of a drug, is a well-established phenomenon which is often accounted for [42]. Physiologically-based pharmacokinetic models

Daniel Câmara De Souza and Morgan Craig are the co-first authors.

Electronic supplementary material The online version of this article (https://doi.org/10.1007/s10928-017-9560-y) contains supplementary material, which is available to authorized users.

✉ Morgan Craig
morganlainecraig@fas.harvard.edu

Daniel Câmara De Souza
daniel.desouza@mail.mcgill.ca

Tyler Cassidy
tyler.cassidy@mail.mcgill.ca

Jun Li
jun.li.2@umontreal.ca

Fahima Nekka
fahima.nekka@umontreal.ca

Jacques Bélair
jacques.belair@umontreal.ca

Antony R. Humphries
tony.humphries@mcgill.ca

[1] Department of Mathematics & Statistics, McGill University, Montreal, QC H3A 0B9, Canada

[2] Program for Evolutionary Dynamics, Harvard University, Cambridge, MA 02138, USA

[3] Faculté de Pharmacie, Université de Montréal, Montreal, QC H3C 3J7, Canada

[4] Département de mathématiques et de statistique, Université de Montréal, Montreal, QC H3C 3J7, Canada

[5] Departments of Mathematics & Statistics, and Physiology, McGill University, Montreal, QC H3A 0B9, Canada

Published online: 13 December 2017

incorporating absorption models like the ACAT or ADAM [2, 25] were indeed conceived and developed in part to account for the enterohepatic circulation that contributes to the delay in drug concentrations in the blood after oral administration. However, regardless of the administration of a xenobiotic, various forms of delays are present throughout physiological systems. In addition to pharmacokinetic lags, systems-level delays play an important role in determining the pharmacodynamic response to treatment. As examples, intracellular and intrinsic viral delays contribute to more complicated viral load decay in patients with human immunodeficiency virus being treated with antiretroviral drugs [16], and the hematopoietic system displays multiple delays along the pathways from the pluripotent hematopoietic stem cells (HSCs) to terminally differentiated circulating cells [31].

Granulopoiesis, the process of neutrophil production, exhibits multiple delays and has been studied in depth owing to the role neutrophils play in the innate (and adaptive) immune response [32]. Neutropenia, a lack of neutrophils, is a toxic side effect of chemotherapy and impacts heavily on treatment success and overall survival outcomes [22, 43]. There is therefore an established interest in mathematical models that can predict the response to chemotherapeutic drugs [17, 20, 40] and accurately represent the feedback mechanisms regulating neutrophil homeostasis [13, 26].

To maintain basal circulating neutrophil concentrations, HSCs become multipotent progenitors in the bone marrow before differentiating into the myeloid lineage on their way to becoming circulating neutrophils. After commitment, cells proliferate and undergo several divisions during a phase where cell numbers increase exponentially. After proliferation, neutrophil progenitors no longer divide. Instead, they grow in size and number of receptors before being sequestered into a marrow reservoir [39], where they either die through apoptosis or transit into circulation [8]. Once they exit from the bone marrow, neutrophils circulate very transiently, with a half-removal time on the order of 7–10 h [48], as they either rapidly die or marginate into tissues [39]. Granulopoiesis is controlled by various cytokines, of which granulocyte colony-stimulating factor (G-CSF) is the principal actor [49]. By binding to receptors on the neutrophil membranes, G-CSF regulates the rate at which neutrophils are released into circulation, and modulates upstream factors (differentiation into the myeloid lineage, proliferation of upstream neutrophil progenitors, speed of maturation) to replenish and regulate the concentration of neutrophils in the bone marrow reservoir. G-CSF is then internalised by the neutrophils and removed from circulation. In the case of elevated circulating concentrations, G-CSF is also cleared via a linear, renal pathway [28] and these dual routes of elimination are important determinants of the PKs of G-CSF [13]. An overview of the process of neutrophil production is given in Fig. 1.

Mathematical representations of granulopoiesis (and other similar physiological delay systems) fall into three classes: transit compartment models where delays are represented via a chain of first-order ordinary differential equations (ODEs), distributed delay systems where integro-differential equations represent a delay that takes a range of values determined through some probability distribution [1, 7, 23, 44], or delay differential equation (DDE) systems where the present state depends on past states via fixed or state-dependent delays [5, 13, 17] (for more detailed discussions on the various models used in modelling hematopoiesis and chemotherapy-induced neutropenia, see [36] and [12], respectively).

Here we focus on two models of granulopoiesis in particular: the Quartino model [38] and the Quantitative systems pharmacology (QSP) model of Craig [13]. The Quartino transit compartment ODE model accounts for the effects and PKs of endogenous G-CSF and is an extension of the widely-used Friberg model [19, 20], while the QSP granulopoiesis model of [13] is a state-dependant delay DDE model that incorporates the concentrations of unbound G-CSF and G-CSF bound to its neutrophil receptors. We will show that the Quartino model [38] can be reformulated as a distributed DDE, which becomes a discrete-delay DDE in a certain parameter limit. This reformulation of the Quartino model leads to some additional insight on parameter choices and will lead us to generalise this model.

Since the maintenance of homeostasis or the pathogenic shift towards disease-states depends on the longterm behaviour of a given system's steady states, stability is an integral concept in physiology. In what follows, we will study the stability of the steady states of these three major granulopoiesis model-types (transit compartment, distributed and discrete delay, and QSP) by demonstrating the relationships and equivalencies between all three formalisms and analysing the resulting distributed delay model to provide a better understanding of the role model selection plays within a treatment context. Accordingly, we will discuss how model choice impacts on the incorporation and delineation of the effects of interindividual variability. We will also provide a historical context for the origins of transit compartment models from distributed delay models and DDEs.

Modelling granulopoiesis: three different approaches to handling delays

Transit compartment model with endogenous G-CSF

The Friberg model [20] is perhaps the most well-known model of chemotherapy-induced myelosuppression in the pharmaceutical sciences [12]. Five compartments are used

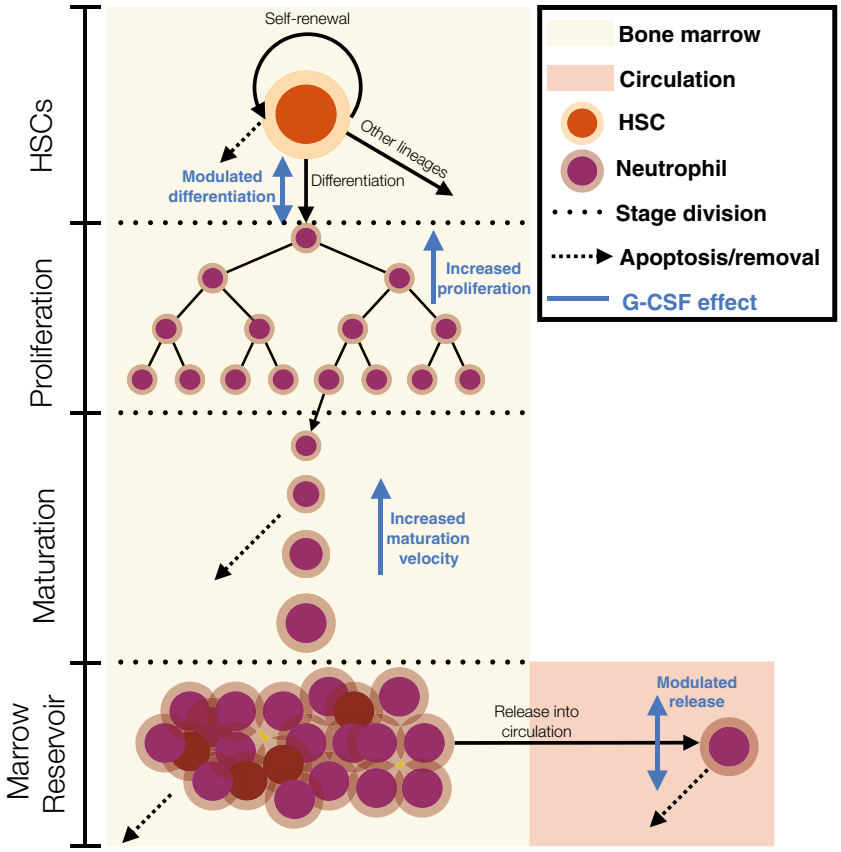

Fig. 1 An overview of granulopoiesis. As with all blood cells, neutrophils begin as hematopoietic stem cells (HSCs–orange circle) in the bone marrow (pale yellow background), where they develop. HSCs are capable of self-renewal and are subject to cell death (dashed arrows). HSCs may also differentiate into one of the blood cell lines, including the neutrophils (purple circles). After commitment to the neutrophil lineage, cells undergo a period of proliferative expansion after which they no longer divide. Post-mitotic neutrophils then mature, growing in size and gaining receptors. At the end of the maturation process, cells are then stored in the bone marrow reservoir from which they egress to reach circulation (pale red background) before removal (by margination or death). G-CSF acts to modulate the rate of exit from the marrow reservoir, increase the rates of maturation and proliferation, and to modulate the rate of differentiation into the neutrophil lineage (G-CSF actions represented by blue vertical arrows). Figure reproduced from: Craig [12] with the permission of Wiley (Color figure online)

to represent the HSCs and early progenitors, circulating neutrophils, and the transit between the proliferative and circulative states. A feedback mechanism on the rate of proliferation determines the extent of myelosuppression of the chemotherapeutic agent. The model has been shown to generically represent a variety of chemotherapeutic drugs [19] and has been widely adopted in PK/PD studies of anti-cancer drugs. We write a generalised version of this model as

$$\begin{aligned}
\frac{dP}{dt} &= \left(k_P(1-E_{Drug})\left(\frac{N_0}{N(t)}\right)^{\gamma} - k_{tr}\right)P \\
\frac{dT_1}{dt} &= k_{tr}P - aT_1 \\
\frac{dT_j}{dt} &= a(T_{j-1} - T_j), \qquad j = 2,\ldots,n \\
\frac{dN}{dt} &= aT_n - k_{circ}N,
\end{aligned} \tag{1}$$

which reduces to the Friberg model if we set $k_P = k_{tr} = a$ and $n = 3$. Here, P is the concentration of proliferating progenitors, T_j is the j^{th} post-mitotic transit compartment, and N is the circulating neutrophil concentration (all in units of 10^9 cells/L), while k_P is the rate of proliferation in the progenitor cell pool, k_{tr} and a are the transit rates between the maturation compartments, and k_{circ} is the rate of neutrophil exit from circulation (all in units of h^{-1}).

An extension to the Friberg model, which we will refer to as the Quartino model, is presented in [38] and models the myelosuppressive effects of chemotherapy on progenitor and circulating neutrophils, the endogenous G-CSF response, and the effect of the administration of a glucocorticoid to induce a rapid increase in G-CSF. A model schematic is given in Fig. 2. For our purposes, we can discount the administration of the glucocorticoid prior to

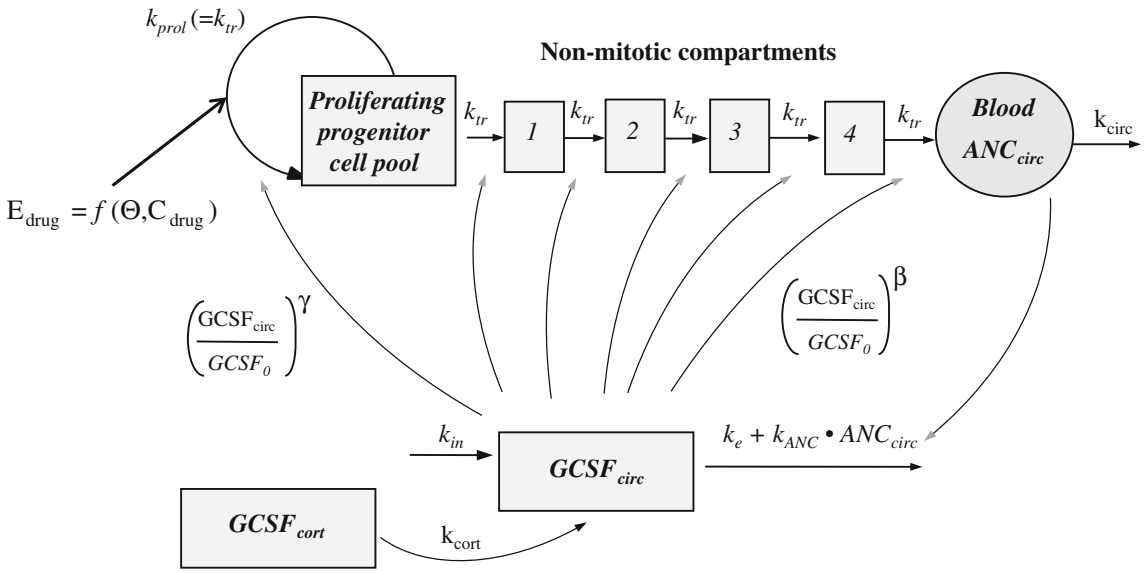

Fig. 2 The integrated G-CSF-myelosuppression model describing the dynamics of endogenous G-CSF and neutrophils following chemotherapy. For the myelosuppression model the parameters are baseline neutrophil count (ANC_0), mean maturation time (MMT = 5/k_{tr}), the half-life of neutrophils in circulation ($t_{1/2_{circ}} = \ln(2)/k_{circ}$), the feedback parameters of G-CSF on neutrophil proliferation (γ) and transit time (β) and the drug related effect (E_{drug}). The estimated parameters for the G-CSF turnover model are baseline G-CSF ($GCSF_0$), nonspecific elimination rate constant (ke) and ANC-dependent elimination rate constant (k_{ANC}) and cortisol-induced G-CSF release (DOSE$cort$) and the half-life of cortisol-induced G-CSF release ($t_{1/2_{cort}} = \ln(2)/k_{cort}$). Figure reproduced from: Quartino et al. [38, p. 3396] with the permission of Springer

chemotherapy and ignore the corresponding model terms. A generalised version of the model is then given by

$$\frac{dP}{dt} = P\left(k_P(1 - E_{Drug})\left(\frac{G}{G_0}\right)^{\gamma} - k_{tr}\left(\frac{G}{G_0}\right)^{\beta}\right) \tag{2a}$$

$$\frac{dT_1}{dt} = \left(\frac{G}{G_0}\right)^{\beta}(k_{tr}P - aT_1) \tag{2b}$$

$$\frac{dT_j}{dt} = a\left(\frac{G}{G_0}\right)^{\beta}(T_{j-1} - T_j), \qquad j = 2, \ldots, n \tag{2c}$$

$$\frac{dN}{dt} = a\left(\frac{G}{G_0}\right)^{\beta} T_n - k_{circ}N \tag{2d}$$

$$\frac{dG}{dt} = k_{in} - (k_e + k_{ANC}N)G, \tag{2e}$$

where G is the circulating G-CSF concentration (ng/L), k_{ANC} is the neutrophil-dependent rate of G-CSF elimination (h^{-1}), k_e is the G-CSF nonspecific elimination rate (h^{-1}), $(G/G_0)^{\gamma}$ is the feedback on the proliferation rate from circulating G-CSF concentrations, and $(G/G_0)^{\beta}$ reflects the G-CSF feedback on the maturation rate.

In most of the current work we do not consider the chemotherapeutic agent and set $E_{Drug} = 0$, unless otherwise stated.

We let P_0, N_0 and G_0 denote the homeostasis values of P, N and G respectively, obtained by setting

$$\frac{dP}{dt} = \frac{dT_j}{dt} = \frac{dN}{dt} = \frac{dG}{dt} = 0 \tag{3}$$

in Eq. (2). In both the Friberg and Quartino models, it is a modelling assumption that

$$k_P = k_{tr}. \tag{4}$$

The condition of Eq. (4) is required in the Friberg model (Eq. 1) to ensure that $N = N_0$ at homeostasis, and in the Quartino model (Eq. 2) to ensure that $G = G_0$ at homeostasis. If G_0 were not the homeostasis value of G, it would be hard to justify the $(G/G_0)^{\beta}$ terms appearing throughout the model, and the model ought to take a different form. Consequently we enforce the condition Eq. (4) throughout, and always assume that $k_{tr} = k_P$ as in [38].

To see why we generalise the model by including a new parameter a, note that at homeostasis the rate of production of proliferating cells, the rate that cells leave proliferation to enter the first transit compartment, the rate they leave the last transit compartment to enter circulation and the rate that they leave circulation must all be equal. In both models this results in

$$k_P P_0 = k_{tr} P_0 = k_{circ} N_0. \tag{5}$$

The production rate in Eq. (5) is completely independent of the maturation time of the cells; provided cells both enter and leave maturation at the rate given by Eq. (5), changing the maturation time τ would only change the total number of cells

that are in maturation (which is $\tau k_P P_0$), but will not change the production rate in Eq. (5). We will see below that at homeostasis the maturation time τ for both models is given by

$$\tau = \frac{n}{a}. \tag{6}$$

Fixing $a = k_{tr}$ leads to two related modelling problems. First if we regard $a = k_{tr}$ as known then, since n is an integer, Eq. (6) only allows for certain discrete values of the delay τ. On the other hand, if as is more usual we suppose that τ is known then choosing n an integer and imposing that $a = k_{tr}$ in Eq. (6) uniquely determines the value of k_{tr} in Eq. (6), which in turn determines the production rate in Eq. (5). But we already noted that the production rate at homeostasis $k_P P_0$ and the maturation time τ are independent.

In Quartino [38] a mean maturation time, or the time it takes cells to transit from the proliferative pool to the circulation, is defined by $MMT = (n+1)/k_{tr}$. Presumably the authors counted n transit compartments plus one proliferation compartment. By showing the equivalence of the generalised Quartino model of Eq. (2) to a distributed DDE, we will find both the mean and variance of the delay, and show that even if $a = k_{tr}$ the correct formula for the mean maturation time should be $MMT = n/k_{tr}$, corresponding to Eq. (6), and not the formula used in Quartino [38].

In the following sections we will consider general values of the parameters a and n, but will take the values of the remaining parameters from [38]; these values are tabulated in Table 1.

To satisfy the homeostasis conditions of Eq. (3) we obtain

$$T_j = \frac{N_0 k_{circ}}{a},\ j = 1, \ldots, n, \qquad P_0 = \frac{N_0 k_{circ}}{k_{tr}}, \tag{7}$$

and the parameter constraint

$$k_{in} = G_0(k_e + k_{ANC} N_0). \tag{8}$$

At homeostasis the total number of cells in the n maturation compartments is $N_0 k_{circ} n/a$. Dividing this by the production rate given by Eq. (5) gives the average maturation time $\tau = n/a$ as stated in Eq. (6).

If $a = k_{tr}$ as in [38] then $T_j = P$ at steady state for all the transit compartments. In [38] the model Eq. (2) is considered with initial conditions at time $t = 0$ equal to the steady-state values (which is natural for a chemotherapy study before the chemotherapeutic agent is administered), but we will consider the behaviour of the model for general non-negative initial conditions.

The linear chain technique

The linear chain technique is used to convert some distributed delay differential equations (DDEs) into a corresponding system of ordinary differential equations (ODEs), or *vice versa*. The technique dates back at least to the work of Vogel in the 1960s [46, 47], and first appears in the English literature in the work of MacDonald [29, 30] who called the method the *linear chain trick*. Most authors continue to use that name, but we prefer *linear chain technique*, because, as we will see, there is a true equivalency between the differential equation systems, and no trick is involved. It is usually more convenient to formulate problems as ODEs for numerical simulation, but sometimes more convenient to formulate them as DDEs for analysis. The linear chain technique is well-known and used in population biology and mathematical epidemiology, but is as yet not as well-known in other fields. The method has been independently rediscovered several times over the decades, being referred to as the fixed boxcartrain method by Goudriaan [21], and recently used by Krzyzanski [27] in a pharmaceutical sciences setting. There are several variants on this technique, and descriptions can be found in many places including [24, 30, 41], but the simplest application is for a gamma distributed delay, for which we will detail the steps here.

Distributed DDEs come in many varieties, but a reasonably general form is

Table 1 Parameter values from [38] for the parameters of interest in this study

Parameter	Description	Units	Typical estimate (% RSE)
N_0	Baseline ANC	10^9 cells/L	3.53 (5)
$k_{tr} = k_P$	Rate of transit	h^{-1}	0.03759
γ	G-CSF feedback on progenitors	–	0.444 (4)
β	G-CSF feedback on maturing cells	–	0.234 (8)
G_0	Baseline G-CSF concentration	ng/L	24.3 (8)
k_e	Non-saturable rate of G-CSF elimination	h^{-1}	0.592 (32)
k_{ANC}	Rate of G-CSF neutrophil removal	$h/10^9$ cells/L	5.64
k_{circ}	Rate of neutrophil removal	h^{-1}	0.099
k_{in}	Rate of G-CSF production	h^{-1}	498.1792

The mean delay in Eq. (29) is given by $\tau = n/a$, or $\tau = 106.4$ h

$$\frac{dN}{dt} = f\left(t, N(t), \int_{-\infty}^{t} P(s) g_a^p(t-s) ds\right) = f\left(t, N(t), \int_0^{\infty} P(t-u) g_a^p(u) du\right). \quad (9)$$

In simpler examples $P(t) \equiv N(t)$, but, as is the case for the models considered in this work, $P(t)$ can also be a separate variable defined by its own differential equation. The function $g_a^p(u)$ is a probability density with

$$\int_0^{\infty} g_a^p(u) du = 1. \quad (10)$$

So, rather than the dynamics of $N(t)$ being determined by the current value of $P(t)$, the integral distributes the effect of P across its previous values. In this work we will restrict attention to the gamma distribution, though other distributions do arise, in particular the uniform distribution. We write the probability density function g_a^p of the gamma distribution as

$$g_a^p(t) = \frac{a^p t^{p-1} e^{-at}}{\Gamma(p)}, \quad (11)$$

where $\Gamma(p)$ is the gamma function. When n is a positive integer $\Gamma(n) = (n-1)!$, and the gamma function generalises the factorial function to real numbers p with $\Gamma(p) = (p-1)\Gamma(p-1)$ for any $p > 0$. The real positive parameters a and p determine the shape and rate of the distribution with the mean delay τ (the delay equation equivalent of the MMT) given by

$$\tau = p/a, \quad (12)$$

and variance $\sigma^2 = p/a^2$. If p and a are taken to infinity with their ratio τ held constant then the variance decreases to zero and the probability density function $g_a^p(t)$ becomes narrower and taller and approaches the δ-function $\delta(t-\tau)$. In this limit the distributed DDE Eq. (9) reduces to a discrete DDE

$$\frac{dN}{dt} = f(t, N(t), P(t-\tau)), \quad (13)$$

so discrete DDEs can be thought of as a limiting case of distributed DDEs. We will see below that when $p = n$ an integer, we can rewrite a gamma distributed DDE as an ODE, so gamma distributed DDEs provide a link between ODEs and discrete DDE models.

Transforming transit compartment models to gamma-distributed delay equations

The probability density function Eq. (11) has the property that for $p \neq 1$

$$\frac{d}{dt} g_a^p(t) = \frac{(p-1)a^p t^{p-2} e^{-at}}{\Gamma(p)} - \frac{a^{p+1} t^{p-1} e^{-at}}{\Gamma(p)} = a\left(\frac{a^{p-1} t^{p-2} e^{-at}}{\Gamma(p-1)} - \frac{a^p t^{p-1} e^{-at}}{\Gamma(p)}\right) = a(g_a^{p-1}(t) - g_a^p(t)). \quad (14)$$

While for $p = 1$

$$\frac{d}{dt} g_a^1(t) = \frac{d}{dt}(a e^{-at}) = -a g_a^1(t). \quad (15)$$

Models of the form in Eqs. (9) and (11) can in principle be considered for any real positive value of p, but in practice nearly all authors only consider $p = n$ a positive integer (one exception is [7]), because then Eqs. (14) and (15) allow the distributed DDE to be reduced to an ODE. To do this for $j = 1, \ldots, n$ let

$$T_j(t) = \int_{-\infty}^{t} P(s) g_a^j(t-s)\, ds = \int_0^{\infty} P(t-u) g_a^j(u)\, du. \quad (16)$$

Then Eq. (9) can be rewritten as an ODE

$$\frac{dN}{dt} = f(t, N(t), T_n(t)). \quad (17)$$

Differentiating Eq. (16), using Leibniz rule for $j > 1$ (noting that $g_a^j(0) = 0$ for $j > 1$) we obtain

$$\frac{dT_j}{dt} = P(t) g_a^j(0) + \int_{-\infty}^{t} P(s) \frac{d}{dt} g_a^j(t-s)\, ds = \int_{-\infty}^{t} P(s) a (g_a^{j-1}(t-s) - g_a^j(t-s))\, ds = a(T_{j-1}(t) - T_j(t)), \quad j = \{2, 3, \ldots, n\}, \quad (18)$$

while for $j = 1$ (noting that $g_a^1(0) = a$)

$$\frac{dT_1}{dt} = P(t) g_a^1(0) + \int_{-\infty}^{t} P(s) \frac{d}{dt} g_a^1(t-s)\, ds = a(P(t) - T_1(t)). \quad (19)$$

Together Eqs. (17), (18), and (19) redefine the (nonlinear) distributed DDE in Eq. (9) as a system of $n+1$ ODEs. General DDEs can be posed as infinite dimensional dynamical systems, which introduces considerable mathematical difficulties, so being able to reduce some DDE models to finite-dimensional ODEs is mathematically very advantageous.

To complete the relationship between the distributed DDE (Eq. (9)) and the system of ODEs in Eqs. (17), (18), and (19) we should take some care with the initial conditions. The distributed DDE (Eq. 9) has infinite memory, and so to solve as an initial value problem from time $t = 0$ we need to define a history function $P(t)$ for all $t \leqslant 0$, so that the right hand-side of Eq. (9) can be evaluated. With

$P(t)$ so defined, for the DDE and ODE reduction to have equivalent solutions, by Eq. (16) the ODE must have initial conditions

$$T_j(0) = \int_{-\infty}^{0} P(s) g_a^j(-s)\, ds = \int_0^{\infty} P(s) g_a^j(s)\, ds \qquad j = 1, \ldots, n. \tag{20}$$

If it is assumed that $P(t) = P_0$, a constant for all $t \leqslant 0$ then, using Eq. (10), we see that Eq. (20) reduces to

$$T_j(0) = P_0 \int_0^{\infty} g_a^j(s)\, ds = P_0, \qquad j = 1, \ldots, n. \tag{21}$$

It is natural to ask if we can also go the other way; does a solution of the system of ODEs Eqs. (17), (18), and (19), define a solution of the distributed DDE in Eq. (9)? It follows immediately from Eq. (21) that a solution of the ODE system with initial conditions $P(0) = T_j(0)$ for $j = 1, \ldots, n$ does define a solution of Eq. (9). The equivalence for more general initial conditions for the ODE has also been established: in that case the ODE initial conditions define a finite number of constraints on the history function $P(t)$ for $t \leqslant 0$, which do not uniquely define $P(t)$, and the ODE defines a solution of the distributed DDE Eq. (9) for all choices of $P(t)$ that satisfy the constraints [10, 30].

Gamma-distributed and discrete delay representations of transit compartment granulopoiesis models

As established above, the linear chain technique can be applied to establish the equivalence between transit compartment ODE models and corresponding distributed DDEs. Consider first the distributed DDE system

$$\begin{aligned} \frac{dP}{dt} &= \left(k_P(1 - E_{Drug}) \left(\frac{N_0}{N(t)} \right)^{\gamma} - k_{tr} \right) P \\ \frac{dN}{dt} &= -k_{circ} N + k_{tr} \int_{-\infty}^{t} P(s) g_a^n(t - s) ds. \end{aligned} \tag{22}$$

We define $T_j(t)$ by

$$T_j(t) = \int_{-\infty}^{t} \frac{k_{tr}}{a} P(s) g_a^j(t - s)\, ds, \qquad j = 1, \ldots, n, \tag{23}$$

which corresponds to Eq. (16) with $k_{tr}P(s)/a$ replacing $P(s)$. Writing the equation for $N(t)$ as

$$\frac{dN}{dt} = -k_{circ} N + a \int_{-\infty}^{t} \frac{k_{tr}}{a} P(s) g_a^n(t - s) ds, \tag{24}$$

and applying the linear chain technique we obtain the generalised Friberg transition compartment model of myelosuppression Eq. (1).

While it is necessary to set $a = k_{tr}$ in Eq. (22) to recover the model as stated in [20], Eq. (1) defines a transit compartment model for other values of a also, and both the system of ODEs in Eq. (1) and the distributed DDE of Eq. (22) can be considered for general values $a > 0$.

The extended Quartino endogenous G-CSF model [38] (Eq. 2) cannot be stated simply as a distributed DDE via the linear chain technique. The maturation time in the Quartino model instead of being constant is state-dependent with the rate constants for the passage through each transit compartment given by

$$a \left(\frac{G(t)}{G_0} \right)^{\beta},$$

which varies as $G(t)$ varies; it reduces to the same value as for the Friberg model only if $G(t) = G_0$.

To write the Quartino model (Eq. 2) as a distributed DDE, we first remove the state-dependency of the delays by rescaling time. Define a new time $\hat{t}(t)$ by

$$\frac{d\hat{t}}{dt} = \left(\frac{G(t)}{G_0} \right)^{\beta}, \qquad \hat{t}(0) = 0. \tag{25}$$

By Theorem 2 in the ESM, the right-hand side of Eq. (25) is strictly positive for $t > 0$ so $\frac{d\hat{t}}{dt} > 0$ and the new time variable $\hat{t}(t)$ is a strictly monotonic increasing function of t. Then we see that

$$\frac{dT_j}{d\hat{t}} = \frac{dt}{d\hat{t}} \frac{dT_j}{dt} = \left(\frac{G_0}{G(\hat{t})} \right)^{\beta} a \left(\frac{G(\hat{t})}{G_0} \right)^{\beta} (T_{j-1} - T_j) = a(T_{j-1} - T_j).$$

Strictly speaking we should define new variables $\widetilde{G}(\hat{t}) = G(t)$, but following common practice we suppress the tildes and reuse the same variable names. Applying the same time-rescaling to all the equations we rewrite the Quartino model (Eq. 2) as

$$\begin{aligned} \frac{dP}{d\hat{t}} &= \left(k_P \left(\frac{G(\hat{t})}{G_0} \right)^{\gamma - \beta} - k_{tr} \right) P(\hat{t}) \\ \frac{dT_1}{d\hat{t}} &= k_{tr} P(\hat{t}) - a T_1(\hat{t}) \\ \frac{dT_j}{d\hat{t}} &= a(T_{j-1}(\hat{t}) - T_j(\hat{t})), \qquad j = 2, \ldots, n \\ \frac{dN}{d\hat{t}} &= a T_n(\hat{t}) - \left(\frac{G_0}{G(\hat{t})} \right)^{\beta} k_{circ} N(\hat{t}) \\ \frac{dG}{d\hat{t}} &= \left(\frac{G_0}{G(\hat{t})} \right)^{\beta} \left(k_{in} - (k_e + k_{ANC} N(\hat{t})) G(\hat{t}) \right). \end{aligned} \tag{26}$$

We refer to Eq. (26) as the time-rescaled Quartino model. Since the time rescaling satisfies $\hat{t}(0) = 0$, the initial conditions for the Quartino model (Eq. 2) at $t = 0$ and the time-rescaled Quartino model (Eq. 26) at time $\hat{t} = 0$ are the same, and these two equations given equivalent solutions.

The time-rescaled Quartino model Eq. (26) has constant transition rates between the transit compartments, and

consequently we can apply the linear chain technique to derive Eq. (26) from

$$\begin{aligned}\frac{\mathrm{d}P}{\mathrm{d}\hat{t}} &= \left(k_P\left(\frac{G(\hat{t})}{G_0}\right)^{\gamma-\beta} - k_{tr}\right)P(\hat{t})\\ \frac{\mathrm{d}N}{\mathrm{d}\hat{t}} &= -\left(\frac{G_0}{G(\hat{t})}\right)^{\beta} k_{circ}N(\hat{t}) + k_{tr}\int_{-\infty}^{\hat{t}} P(s)g_a^n(\hat{t}-s)\,ds \qquad (27)\\ \frac{\mathrm{d}G}{\mathrm{d}\hat{t}} &= \left(\frac{G_0}{G(\hat{t})}\right)^{\beta}\Big(k_{in} - (k_e + k_{ANC}N(\hat{t}))G(\hat{t})\Big),\end{aligned}$$

by letting

$$T_j(\hat{t}) = \int_{-\infty}^{\hat{t}} \frac{k_{tr}}{a}P(s)g_a^j(\hat{t}-s)\,ds, \qquad j = 1,\ldots,n. \qquad (28)$$

To define an initial value problem for the distributed DDE of Eq. (27) we need to specify $N(0)$, $G(0)$ and $P(\hat{t})$ for $\hat{t} \leqslant 0$. This in turn defines initial conditions for both the time-rescaled Quartino model Eq. (26) and the Quartino model of Eq. (2) with $T_j(0)$ given by evaluating Eq. (28) with $\hat{t} = 0$. If $P(\hat{t})$ is constant for $\hat{t} \leqslant 0$ then Eq. (28) implies that $T_j(0) = k_{tr}P(0)/a$, so there is an immediate equivalence between all three models for such initial conditions. Even if the Quartino model Eq. (2) were considered with different initial conditions, there is still a direct equivalence to the time-rescaled Quartino model (Eq. 26) and to the distributed DDE model (Eq. 27). Consequently we have three equivalent forms of the same model, with a direct correspondence between the solutions of the differential equation systems Eqs. (2) and (26) and (27).

Recalling Eq. (12), the mean value of the distributed delay in Eq. (27) is $\tau = n/a$. The time rescaling Eq. (25) is trivial at homeostasis when $G(t) = G_0$, so this also implies that the mean maturation delay is $\tau = n/a$ in the Quartino model Eq. (2).

Fixing $a = k_{tr}$ would only allow a very granular control of the mean delay in the ODE model by varying the integer n. Mathematically it is more convenient to fix the delay $\tau > 0$ and use n and a to control the shape of the distribution. For the distributed DDE model (Eq. 27) we do not even need n to be an integer. Recalling Eq. (10), in the limit as $n \to \infty$ and $a \to \infty$ with $\tau = n/a$ fixed, the distributed DDE (Eq. 27) reduces to the discrete DDE

$$\begin{aligned}\frac{\mathrm{d}P}{\mathrm{d}\hat{t}} &= \left(k_P\left(\frac{G(\hat{t})}{G_0}\right)^{\gamma-\beta} - k_{tr}\right)P(\hat{t})\\ \frac{\mathrm{d}N}{\mathrm{d}\hat{t}} &= -\left(\frac{G_0}{G(\hat{t})}\right)^{\beta} k_{circ}N(\hat{t}) + k_{tr}P(\hat{t}-\tau) \qquad (29)\\ \frac{\mathrm{d}G}{\mathrm{d}\hat{t}} &= \left(\frac{G_0}{G(\hat{t})}\right)^{\beta}\Big(k_{in} - (k_e + k_{ANC}N(\hat{t}))G(\hat{t})\Big).\end{aligned}$$

We remark that in the discrete DDE Eq. (29) the delay τ is constant in the rescaled time-variable $\hat{t}$, just as the (same) mean delay $\tau = n/a$ is constant in the distributed DDE Eq. (27). In contrast the mean maturation time $\alpha(t)$ in the Quartino model of Eq. (2) varies with $G(t)$ and satisfies

$$\hat{t}(t - \alpha(t)) = \hat{t}(t) - \tau,$$

where $\hat{t}(t)$ satisfies Eq. (25). If G is held constant (but not necessarily equal to G_0), this gives a mean maturation time α in the Quartino model Eq. (2) of

$$\alpha = \frac{n}{a(G/G_0)^{\beta}} = \frac{\tau}{(G/G_0)^{\beta}}.$$

For the case of time-varying $G(t)$, the evolution of the mean maturation delay $\alpha(t)$ is defined by the differential Eq. (A2), which we derive in the ESM, where we also show the similarities between this state-dependency and the explicit state-dependency in the QSP model (Eq. 30). But, in the current work, the time-rescaling Eq. (25) will be sufficient for our purposes.

Since the system in Eq. (26) corresponds to the Quartino model in Eq. (2) with time rescaled, positivity of solutions is guaranteed by Theorem 2 in the ESM.

A QSP model of granulopoiesis and its regulation by G-CSF

As previously mentioned, DDEs are frequently relied upon to model granulopoiesis given the delays inherent to hematopoiesis. Here we focus on the Quantitative Systems Pharmacology model in [13], which has been shown to account for the dynamics of neutrophil production and its negative feedback relationship with G-CSF–both bound to receptors on the surface of neutrophils and freely circulating–in a variety of scenarios. The model is written as

$$\begin{aligned}\frac{\mathrm{d}}{\mathrm{d}t}Q(t) &= -\big(\kappa(G_1(t)) + \kappa_\delta + \beta(Q(t))\big)Q(t)\\ &\quad + A_Q(t)\beta(Q(t-\tau_Q))Q(t-\tau_Q) \qquad (30a)\\ \frac{\mathrm{d}}{\mathrm{d}t}N_R(t) &= A_N(t)\kappa(G_1(t-\tau_N(t)))\\ &\quad \times Q(t-\tau_N(t))\frac{V_{N_M}(G_1(t))}{V_{N_M}(G_1(t-\tau_{N_M}(t)))}\\ &\quad - \big(\gamma_{N_R} + \varphi_{N_R}(G_{BF}(t))\big)N_R(t) \qquad (30b)\\ \frac{\mathrm{d}}{\mathrm{d}t}N(t) &= \varphi_{N_R}(G_{BF}(t))N_R(t) - \gamma_N N(t), \qquad (30c)\\ \frac{\mathrm{d}}{\mathrm{d}t}G_1(t) &= I_G(t) + G_{prod} - k_{ren}G_1(t) \qquad (30d)\\ &-k_{12}([N_R(t) + N(t)]V - G_2(t))G_1(t)^{s_G} + k_{21}G_2(t) \qquad (30e)\end{aligned}$$

$$\frac{\mathrm{d}}{\mathrm{d}t}G_2(t) = -k_{int}G_2(t) + k_{12}\big([N_R(t)+N(t)]V - G_2(t)\big)G_1(t)^{s_G} - k_{21}G_2(t). \tag{30f}$$

Here $Q(t)$ is the concentration of HSCs (10^6 cells/kg), $N_R(t)$ the concentration of neutrophils in the bone marrow reservoir (10^9 cells/kg), $N(t)$ the concentration of circulating neutrophils (10^9 cells/kg), $G_1(t)$ the circulating G-CSF concentration (ng/mL), and $G_2(t)$ the bound G-CSF concentration (ng/mL). Here, and throughout, the superscript ^{h} denotes the homeostasis value of a quantity. The QSP model (Eq. 30) is subject to the initial conditions (ICs) and history functions

$$\begin{aligned} Q(s) &= \varphi_1(s) \quad \text{for s} \in [-\tau_Q, 0] \\ N_R(0) &= N_{R,0} \\ N(0) &= N_0 \\ G_1(s) &= \varphi_2(s) \quad \text{for s} \in [-\tau, 0] \\ G_2(0) &= G_{2,0}, \end{aligned} \tag{31}$$

where $\varphi_{1,2}(t) \in \mathcal{C}^0$ and

$$\tau = \sup_{t\geqslant 0} \tau_N(t). \tag{32}$$

$I_G(t)$ models the administration of exogenous G-CSF. As described in [13], the self-renewal $\beta(Q)$ and amplification factor $A_Q(t)$ of the HSCs are given by

$$\beta(Q) = f_Q \frac{\theta_2^{s_Q}}{\theta_2^{s_Q} + Q^{s_Q}}, \qquad A_Q(t) = A_Q^h = 2e^{-\gamma_Q \tau_Q},$$

and the rate at which HSCs differentiate into neutrophil precursors is determined by the circulating concentration of G-CSF

$$\kappa(G_1) = \kappa^h + (\kappa^h - \kappa^{min})\left[\frac{G_1^{s_\kappa} - (G_1^h)^{s_\kappa}}{G_1^{s_\kappa} + (G_1^h)^{s_\kappa}}\right].$$

The rate at which the neutrophil progenitors proliferate is given by

$$\eta_{N_P}(G_1(t)) = \eta_{N_P}^h + (\eta_{N_P}^h - \eta_{N_P}^{min})\frac{b_{N_P}}{G_1^h}\left(\frac{G_1(t) - G_1^h}{G_1(t) + b_{N_P}}\right), \tag{33}$$

where τ_{N_P} days is the time it takes for proliferation. After exiting proliferation, cells mature with rate

$$V_{N_M}(G_1(t)) = 1 + (V_{max} - 1)\frac{G_1(t) - G_1^h}{G_1(t) - G_1^h + b_V},$$

where the maximal age of maturing neutrophils is a_{N_M}. Given $V_{N_M}(G_1(t))$ depends on the circulating concentration of G-CSF, the time it takes neutrophils to mature satisfies

$$\int_{t-\tau_{N_M}(t)}^{t} V_{N_M}(G_1(s))ds = a_{N_M}, \tag{34}$$

and the total time for the process of granulopoiesis is then the sum of the time to completion of each process, given by

$$\tau_N(t) = \tau_{N_P} + \tau_{N_M}(t).$$

Maturing neutrophils are assumed to be subject to a constant death rate γ_{N_M}, and their amplification factor $A_N(t)$ is given by the integral equation

$$A_N(t) = \exp\left[\int_{t-\tau_N(t)}^{t-\tau_{N_M}(t)} \eta_{N_P}(G_1(s))ds - \gamma_{N_M}\tau_{N_M}(t)\right]. \tag{35}$$

The fraction of G-CSF bound to neutrophil receptors given by

$$G_{BF}(t) = \frac{G_2(t)}{V[N_R(t) + N(t)]} \in [0,1], \qquad G_{BF}^h = \frac{G_2^h}{V[N_R^h + N^h]}.$$

regulates the rate with which cells exit the marrow reservoir as

$$\varphi_{N_R}(G_{BF}(t)) = \varphi_{N_R}^h + (\varphi_{N_R}^{max} - \varphi_{N_R}^h)\frac{G_{BF}(t) - G_{BF}^h}{G_{BF}(t) - G_{BF}^h + b_G}.$$

Mature neutrophils die from the marrow reservoir with rate γ_{N_R}. Cells that transit into circulation are removed with constant rate γ_N.

Proofs of the existence, uniqueness, positivity, and boundedness of solutions to Eq. (30) are provided in the ESM.

Stability analysis

We perform stability analyses of the models highlighted above by linearising them about their equilibria and investigating the roots of the associated characteristic equations. As in the methodology familiar to systems of ODEs, where characteristic equations are polynomial, we will calculate the parameter values for which the roots have positive real parts, corresponding to an unstable equilibrium.

In general, the characteristic equation associated with an arbitrary distribution is transcendental and possesses an infinite number of roots. As we shall see, the advantage of an integer-order gamma distribution is to yield a characteristic equation which is also a polynomial, reflecting the fact that the gamma distribution yields a system of ODEs. In the context of comparing and contrasting the different models, we obtain a "continuity" result of sorts as we determine that approximation in distribution does lead to approximation in stability diagrams (see [3] for a similar continuity argument).

Stability analysis for the Quartino endogenous G-CSF model and related forms

The generalised Quartino model Eq. (2), has two steady states. Assuming that $k_{tr} = k_P$ as in Eq. (4) for the reasons already stated, and considering the model in the form Eq. (41) with vector solution $\mathbf{X}(t) = (P(t), T_1(t), \ldots, T_n(t), N(t), G(t)) \in \mathbb{R}^n$ these are given by

$$\mathbf{X}_1^* = [P, T_1, \ldots, T_n, N, G] = \left[0, 0, \ldots, 0, 0, \frac{k_{in}}{k_e}\right], \tag{36}$$

$$\mathbf{X}_2^* = \left[\frac{k_{circ} N_0}{k_{tr}}, \frac{k_{circ} N_0}{a}, \ldots, \frac{k_{circ} N_0}{a}, N_0, G_0\right], \tag{37}$$

where N_0 is given by Eq. (8). The time-rescaled Quartino model (Eq. 26) has the same steady states $\mathbf{X}_1^*$ and $\mathbf{X}_2^*$, since a monotonic rescaling of time does not affect equilibria.

The discrete and distributed Quartino DDE models have related equilibria, but in fewer space dimensions, since these models do not include transit compartments. Let $\mathbf{Y}(\hat{t}) = (P(\hat{t}), N(\hat{t}), G(\hat{t}))^\intercal \in \mathbb{R}^3$ denote the vector of solutions of Eq. (27) or (29), then these steady states are given by

$$\mathbf{Y}_1^* = \left[0, 0, \frac{k_{in}}{k_e}\right], \tag{38}$$

$$\mathbf{Y}_2^* = \left[\frac{k_{circ} N_0}{k_{tr}}, N_0, G_0\right]. \tag{39}$$

If n is a positive integer the distributed DDE (Eq. 27) is equivalent to the Quartino model (Eq. 2) and the steady states $\mathbf{Y}_1^*$ and $\mathbf{Y}_2^*$ correspond exactly to $\mathbf{X}_1^*$ and $\mathbf{X}_2^*$ as defined in Eqs. (36) and (37) for the same value of n, and with the values of T_j following from Eq. (28). To study the stability of $\mathbf{X}_i^*$ and $\mathbf{Y}_i^*$, we construct characteristic equations for the Quartino endogenous G-CSF models.

Consider first the generalised Quartino model (Eq. 2). Let

$$\mathbf{X}(t) := (P(t), T_1(t), \ldots, T_n(t), N(t), G(t))^\intercal \in \mathbb{R}^{n+3} \tag{40}$$

be the vector of solutions so that Eq. (2) can be rewritten in vector form as

$$\frac{\mathrm{d}\mathbf{X}}{\mathrm{d}t} = \mathbf{F}(\mathbf{X}), \tag{41}$$

where $\mathbf{F}(\mathbf{X})$ represents the right hand side of the Quartino model (Eq. 2). Let $\mathbf{X}^*$ be an equilibrium of the system (that is that $\mathbf{F}(\mathbf{X}^*) = 0$), then define $\mathbf{Z} = \mathbf{X}(t) - \mathbf{X}^*$ and let $\mathbb{J}(\mathbf{X}^*)$ be the Jacobian of $\mathbf{F}(\mathbf{X})$ evaluated at $\mathbf{X}^*$ ($\mathbb{J}(\mathbf{X}) = d\mathbf{F}/d\mathbf{X}$). Then linearising about $\mathbf{X}^*$ we obtain

$$\frac{\mathrm{d}\mathbf{Z}}{\mathrm{d}t} = \mathbb{J}(\mathbf{X}^*)\mathbf{Z}, \tag{42}$$

where nonlinear terms of order $\mathcal{O}(\|\mathbf{Z}\|^2)$ are neglected. Seeking a nontrivial exponential solution $\mathbf{Z}(t) = \mathbf{C}e^{\lambda t}$ of Eq. (42) with $\mathbf{C} \in \mathbb{R}^{n+3}$, a vector of constants, and $\lambda \in \mathbb{C}$, we obtain the characteristic equation

$$\det(\lambda \mathbb{I} - \mathbb{J}) = 0, \tag{43}$$

where $\mathbb{I} \in \mathbb{R}^{(n+3)\times(n+3)}$ is the identity matrix. Evaluating the determinant in Eq. (43) leads to the characteristic equation, which is stated in Eq. (A15) in the Electronic Supplementary Material. This gives a polynomial of degree $n + 3$ in λ for the Quartino model Eq. (2), and a polynomial of degree 7 if we set $n = 4$, as in [38]. A steady state is unstable if any of the roots of this polynomial have positive real part.

The characteristic polynomial for the time rescaled Quartino model is also a polynomial in λ of degree $n + 3$, and actually has a simpler form than the characteristic polynomial for Quartino model Eq. (2). But to derive this characteristic polynomial it is convenient to first consider the characteristic functions of the discrete DDE (Eq. 29) and the distributed DDE model (Eq. 27).

With $\mathbf{Y}(\hat{t})$ defined as above, let $\mathbf{Y}_\tau := \mathbf{Y}(\hat{t} - \tau)$ be the vector of delayed solutions. Then we can rewrite Eq. (29) as

$$\frac{\mathrm{d}\mathbf{Y}}{\mathrm{d}\hat{t}} = \mathbf{F}(\mathbf{Y}, \mathbf{Y}_\tau), \tag{44}$$

in vector form. Similar to the ODE case, let $\mathbf{F}(\mathbf{Y}^*, \mathbf{Y}^*) = \mathbf{0}$ be a generic steady state. Define the variables $\mathbf{Z} := \mathbf{Y} - \mathbf{Y}^*$ and $\mathbf{Z}_\tau := \mathbf{Y}_\tau - \mathbf{Y}^*$ and denote the linearisation matrices of Eq. (44) computed at $(\mathbf{Y}, \mathbf{Y}_\tau) = (\mathbf{Y}^*, \mathbf{Y}^*)$ by $\mathbb{A}$ and $\mathbb{B}$. Linearising Eq. (44) about $\mathbf{Y}^*$ and using the variables $\mathbf{Z}$ and $\mathbf{Z}_\tau$ yields

$$\frac{\mathrm{d}\mathbf{Z}}{\mathrm{d}\hat{t}} = \mathbb{A}\mathbf{Z} + \mathbb{B}\mathbf{Z}_\tau. \tag{45}$$

The linearisation matrices $\mathbb{A}$ and $\mathbb{B}$ from Eq. (45) are calculated following Eq. (A22) in the ESM. Seeking a nontrivial exponential solution $\mathbf{Z}(t) = \mathbf{C}e^{\lambda \hat{t}}$ for Eq. (45), with constant $\mathbf{C} \in \mathbb{R}^3$ and $\lambda \in \mathbb{C}$, we obtain the characteristic equation

$$\det(\lambda \mathbb{I} - \mathbb{A} - e^{-\lambda\tau}\mathbb{B}) = 0, \tag{46}$$

where $\mathbb{I}$ is the identity matrix. Evaluating the determinant in Eq. (46) gives the transcendental characteristic equation

$$\lambda^3 + a_2\lambda^2 + a_1\lambda + a_0 = be^{-\lambda\tau}, \tag{47}$$

where the coefficients a_2, a_1, a_0 and b are computed in Eq. (A23) (see ESM).

In general Eq. (47) has infinitely many roots, corresponding to the infinite dimensional nature of DDEs. The treatment of these equations is made tractable because although there can be infinitely many complex numbers λ

that satisfy Eq. (47), it is well known that for any real number σ there can only be finitely many solutions λ with $Re(\lambda) > \sigma$ (see for example Lemma 4.2 in [41]). To determine stability we need to ascertain whether all the roots have $Re(\lambda) < 0$.

Comparing the discrete DDE in Eq. (29) with the distributed DDE in Eq. (27), we see that they differ in only one term. Thus the linearisation of the distributed DDE (27) follows exactly the steps taken for the discrete DDE (29). Then, following MacDonald [30], the characteristic equation for the distributed DDE of Eq. (27) corresponds to Eq. (47) with the term $e^{-\lambda\tau}$ replaced by

$$G(\lambda) = \int_0^\infty e^{-\lambda u} g_a^n(u) du = \frac{a^n}{(a+\lambda)^n}, \tag{48}$$

where $G(\lambda)$ is the Laplace transform of the gamma probability density function, and hence we obtain

$$\lambda^3 + a_2\lambda^2 + a_1\lambda + a_0 - \frac{a^n b}{(a+\lambda)^n} = 0, \tag{49}$$

where the coefficients a_j and b computed in Eq. (A23) in the ESM are the same as those for Eq. (47). Notice that if $b = 0$ then Eqs. (47) and (49) both reduce to the same cubic polynomial.

Equation (49) is the characteristic equation of both the distributed DDE (Eq. 27) and the equivalent time-rescaled Quartino ODE model (Eq. 26), and can be written as

$$(1 + \lambda/a)^n(\lambda^3 + a_2\lambda^2 + a_1\lambda + a_0) - b = 0, \tag{50}$$

a polynomial of degree $n + 3$, for $b \neq 0$. The above equation can be used to determine the stability of the steady-states of these models. But since the time rescaling Eq. (25) is monotonic this will also determine the stability of the steady-states of the Quartino model (Eq. 2).

It is natural to think of the discrete DDE (Eq. 29) as the limit as $n \to \infty$ with $a = n/\tau$ of the distributed DDE (Eq. 27), and indeed with $a = n/\tau$ we have

$$(1 + \lambda/a)^n = (1 + \lambda\tau/n)^n \;\to\; e^{\lambda\tau} \text{ as n} \to \infty, \tag{51}$$

so the characteristic Eq. (50) for the distributed DDE approaches the characteristic Eq. (47) of the discrete DDE as $n \to \infty$.

With the characteristic equations at hand, we now state the stability results for the Quartino endogenous G-CSF model and related forms. The complete proof is provided in the ESM and is sketched out here. We can also directly derive stability results for the Quartino model for at least the steady state $\mathbf{X}_1^*$, though the proofs are much more involved; those results, along with the requisite proof of the positivity of solutions, are provided in the ESM for completeness.

Theorem 1 *Provided the parameters satisfy the constraints* (4) *and* (8)

1. *For the distributed DDE in Eq.* (27) *and the discrete DDE of Eq.* (29) *the steady state* $\mathbf{Y}_1^*$ *is locally asymptotically stable if* $\gamma < \beta$ *and unstable if* $\gamma > \beta$, *and the steady state* $\mathbf{Y}_2^*$ *is unstable if* $\gamma < \beta$.
2. *For the Quartino model in Eq.* (2) *and the time rescaled Quartino model in Eq.* (26) *the steady state* $\mathbf{X}_1^*$ *is locally asymptotically stable if* $\gamma < \beta$ *and unstable if* $\gamma > \beta$, *and the steady state* $\mathbf{X}_2^*$ *is unstable if* $\gamma < \beta$.

Sketch of proof The DDEs considered here are examples of retarded functional differential equations (RFDEs). For RFDEs, it is a standard result that the stability of steady states is determined by the linearization; see for example Theorem 4.8 in [41]. Stability is then shown by considering the characteristic equations. $\mathbf{Y}_1^*$ can be shown to be unstable for $\gamma > \beta$ by the intermediate value theorem, and similarly for $\mathbf{Y}_2^*$ when $\gamma < \beta$. The Routh-Hurwitz criteria can be used to show the stability of $\mathbf{Y}_1^*$ when $\gamma < \beta$. Results for $\mathbf{X}_j^*$ follow from those for $\mathbf{Y}_j^*$. □

For the standard parameters, as given in Table 1, we have $\gamma > \beta$ so Theorem 1 implies that the neutropenic steady states $\mathbf{X}_1^*$ and $\mathbf{Y}_1^*$ are unstable in all these models. Proving directly that the homeostatic steady states $\mathbf{X}_2^*$ and/or $\mathbf{Y}_2^*$ are stable when $\gamma > \beta$ is difficult, but we can compute the roots of the characteristic equations, and these are shown in Fig. 3. We see that all the roots are negative or have negative real part and hence the homeostatic steady states $\mathbf{X}_2^*$ and $\mathbf{Y}_2^*$ are indeed stable when $\gamma > \beta$. Moreover, the characteristic roots for the time-rescaled transit compartment Quartino model converge to the characteristic roots for the discrete DDE as n increases. Although the steady state is stable for all the models, we see that it becomes less stable as n increases, with the real part of the characteristic values tending to increase with n. The phenomenon of loss of stability for fixed delay τ as n is increased has long been known, but remains an area of active interest [4, 7, 30]. However, when $\gamma = \beta$ the model is degenerate with the progenitor equation reducing to $\frac{dP}{dt} = 0$, so the change in stability observed in Theorem 1 depending on whether $\gamma > \beta$ or $\gamma < \beta$ is *not* a bifurcation in the usual sense.

Stability of the QSP model of granulopoiesis

Similar to the preceding analysis, let $\mathbf{X}(t) := (Q(t), N_R(t), N(t), G_1(t), G_2(t))^\intercal$ be the vector solution of Eq. (30) and $\mathbf{X}_\sigma := \mathbf{X}(t - \sigma)$ denote a vector of delayed solutions. Then the DDE system defining the QSP model (Eq. 30) can be rewritten in vector form as

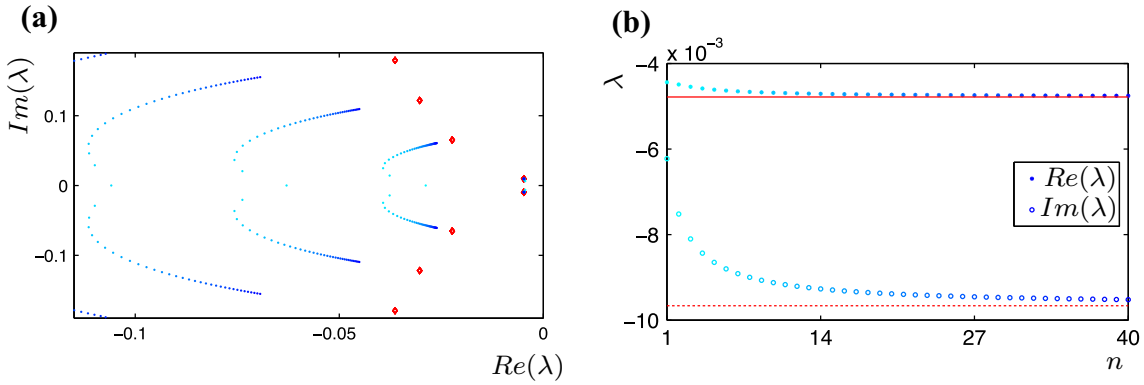

Fig. 3 Convergence of the characteristic roots. Characteristic roots for the distributed DDE (Eq. 27) at $\mathbf{Y}_2^*$ and the equivalent time-rescaled Quartino model (Eq. 26) at $\mathbf{X}_2^*$ are both given by solutions of Eq. (49). Characteristic roots transition from cyan to blue as n is increased from 1 to 40 (see online version for colours). As n is increased the roots are seen to converge to the characteristic roots at $\mathbf{Y}_2^*$ of the discrete DDE (Eq. 29) which are given by Eq. (47). **a** In the complex plane. Diamonds: Characteristic roots of Eq. (47); Dots: Characteristic roots of Eq. (49) as n is varied. **b** Convergence of the real and negative imaginary part of the rightmost characteristic root of Eq. (49) to the corresponding root of Eq. (47) as n is increased (Color figure online)

$$\frac{\mathrm{d}\mathbf{X}}{\mathrm{d}t} = \mathbf{F}(\mathbf{X}, \mathbf{X}_{\tau_Q}, \mathbf{X}_{\tau_N}, \mathbf{X}_{\tau_{N_M}}). \tag{52}$$

Parameters changes to the model lead to different steady states in Eq. (52). Let the steady state computed at homeostasis be written as $\mathbf{X}^h \equiv (Q^h, N_R^h, N^h, G_1^h, G_2^h)$, and denote a generic steady state by $\mathbf{X}^* \equiv (Q^*, N_R^*, N^*, G_1^*, G_2^*)$.

To linearize Eq. (52) around a steady state $\mathbf{X}^*$ we define the variables $\tau(t) = \tau_N(t) - t$ and $u = s + \tau(t)$ to rewrite the amplification factor Eq. (35) as

$$A_N(t) = \exp\left[\int_0^{\tau_{N_P}} \eta_{N_P}(G_1(u - \tau(t)))du - \gamma_{N_M}\tau_{N_M}(t)\right]. \tag{53}$$

Thus we approximate the amplification factor Eq. (53) through the linearisation of the proliferation function Eq. (33) given by

$$\eta_{N_P}(G_1) = \eta_{N_P}(G_1^*) + \eta'_{N_P}(G_1^*)(G_1 - G_1^*) + \mathcal{O}(|G_1 - G_1^*|^2), \tag{54}$$

where $\eta'_{N_P} \equiv d\eta_{N_P}/dG_1$. Further, since it does not affect the local stability of the steady state [11], we freeze the state-dependent delay at its steady state value

$$\tau_{N_M}(t) = \tau_{N_M}^*. \tag{55}$$

Using Eqs. (54) and (55) together with the distributed delay variable defined by

$$\tilde{G}_1(t) := \int_0^{\tau_{N_P}} \frac{G_1(u - \tau(t))}{\tau_{N_P}} du,$$

Eq. (53) becomes

$$\tilde{A}_N(t) = \exp\left[\eta_{N_P}^*\tau_{N_P} - \gamma_{N_M}\tau_{N_M}^* + \eta'_{N_P}(G_1^*)\tau_{N_P}(\tilde{G}_1(t) - G_1^*)\right]. \tag{56}$$

As a consequence of the approximation in Eq. (56), we can rewrite Eq. (52) as

$$\frac{\mathrm{d}\mathbf{X}}{\mathrm{d}t} = \mathbf{f}(\mathbf{X}, \mathbf{X}_{\tau_Q}, \mathbf{X}_{\tau_N}, \mathbf{X}_{\tau_{N_M}}, \tilde{\mathbf{X}}), \tag{57}$$

where

$$\tilde{\mathbf{X}}(t) := \int_0^{\tau_{N_P}} \frac{\mathbf{X}(u - \tau(t))}{\tau_{N_P}} du.$$

Let $\mathbf{X}^*$ be a generic steady state of Eq. (57), defined by $\mathbf{f}(\mathbf{X}^*, \mathbf{X}^*, \mathbf{X}^*, \mathbf{X}^*, \mathbf{X}^*) = \mathbf{0}$. Define the variables $\mathbf{Z} := \mathbf{X} - \mathbf{X}^*$, $\mathbf{Z}_\sigma := \mathbf{X}_\sigma - \mathbf{X}^*$ and $\tilde{\mathbf{Z}} := \tilde{\mathbf{X}} - \mathbf{X}^*$ and denote the linearisation matrices of Eq. (57) with regards to $\mathbf{X}$, $\mathbf{X}_{\tau_Q}$, $\mathbf{X}_{\tau_N}$, $\mathbf{X}_{\tau_{N_M}}$, $\mathbf{X}_\tau$ and computed at $\mathbf{X}^*$, respectively by $\mathbb{A}$, $\mathbb{B}$, …, $\mathbb{E}$. Linearising Eq. (57) about $\mathbf{X}^*$ and using the variables $\mathbf{Z}$, $\mathbf{Z}_\sigma$ and $\tilde{\mathbf{Z}}$ yields

$$\frac{\mathrm{d}\mathbf{Z}}{\mathrm{d}t} = \mathbb{A}\mathbf{Z} + \mathbb{B}\mathbf{Z}_{\tau_Q} + \mathbb{C}\mathbf{Z}_{\tau_N} + \mathbb{D}\mathbf{Z}_{\tau_{N_M}} + \mathbb{E}\tilde{\mathbf{Z}}. \tag{58}$$

The linearisation matrices $\mathbb{A}$, $\mathbb{B}$, …, $\mathbb{E}$ from Eq. (58) are computed in Eq. (A26) and Eq. (A27) in the ESM. Seeking a nontrivial exponential solution $\mathbf{Z}(t) = \mathbf{C}e^{\lambda t}$ for Eq. (58), with constant $\mathbf{C} \in \mathbb{R}^5$ and $\lambda \in \mathbb{C}$, we obtain the characteristic equation

$$\det(\lambda\mathbb{I} - \mathbb{A} - e^{-\lambda\tau_Q}\mathbb{B} - e^{-\lambda\tau_N^*}\mathbb{C} - e^{-\lambda\tau_{N_M}^*}\mathbb{D} - f(\lambda)\mathbb{E}) = 0, \tag{59}$$

where $\mathbb{I}$ is the identity matrix and

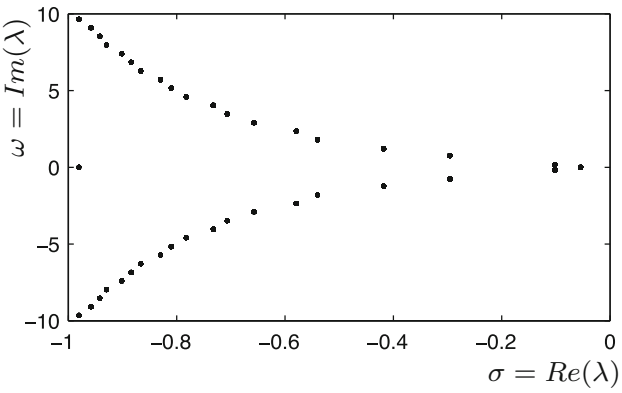

Fig. 4 Roots of the characteristic equation Eq. (59) of the QSP granulopoiesis model (Eq. 30) evaluated at the homeostasis steady state $\mathbf{X}^h$. All roots have negative real part in the complex plane

$$f(\lambda) := \frac{(e^{\lambda\tau_{N_P}} - 1)}{\lambda\tau_{N_P} e^{\lambda\tau_N^*}} = \frac{e^{-\lambda\tau_{N_M}^*} - e^{-\lambda\tau_N^*}}{\lambda\tau_{N_P}}. \tag{60}$$

See the calculations following Eq. (A26) and Eq. (A27) in the ESM for the rearrangement of Eq. (59), and computation of the matrix terms and its determinant. The characteristic roots, solutions $\lambda \in \mathbb{C}$ to Eq. (59), determine the stability of the steady state $\mathbf{X}^*$ from Eq. (52)/(58). To evaluate the stability numerically, we write $\lambda = \sigma + i\omega$, with $\sigma \in \mathbb{R}$ and $\omega \in \mathbb{R}$, and then compute the roots of Eq. (59) in the (σ, ω)-plane using the Matlab subroutine *fsolve* [33]. As illustrated in Fig. 4, at homeostasis all the characteristic roots λ have negative real part, and so the homeostatic steady state $\mathbf{X}^h = (Q^h, N_R^h, N^h, G_1^h, G_2^h)$, defined by $\mathbf{F}(\mathbf{X}^h, \mathbf{X}^h, \mathbf{X}^h, \mathbf{X}^h) = \mathbf{0}$ in Eq. (52) is locally asymptotically stable.

Bifurcation studies

Bifurcation analysis, or the study of the qualitative changes to the behaviour of a system given a change to parameter values, is a fundamental dynamical systems concept [34]. Accordingly, it can be a powerful tool in the life sciences to shed light on underlying parameter relationships and better understand the robustness of a system with regards to stability.

Historically, bifurcation analysis has been applied to study hematological pathologies and has provided valuable insight into the origins of disorders like cyclic neutropenia, a disease associated with dangerously low neutrophil counts and mouth blistering [14] where a patient's ANCs oscillate with a period of around 21 days. These oscillations have been shown to correspond to a periodic orbit that appears through a loss of stability after the system undergoes a Hopf bifurcation [9, 18].

Bifurcations in the equivalent expressions of the Quartino endogenous G-CSF model

We begin by investigating whether parameter changes in the equivalent expressions of the Quartino endogenous G-CSF model can lead their steady states $\mathbf{X}_2^*$ and $\mathbf{Y}_2^*$ to lose stability. As in the homeostatic case, we let $\lambda = \sigma + i\omega$, and compute the roots of the characteristic equations Eqs. (47), (49) and (A19) using the Matlab subroutines *roots* and *fsolve* [33]. We only consider the parameter regime where $\gamma > \beta$ as this includes the homeostatic steady states and avoids the model degeneracy that occurs when $\gamma = \beta$. Given that our aim is to compare the various models, we will not perform an exhaustive study of the effects of varying all the parameters here, but restrict

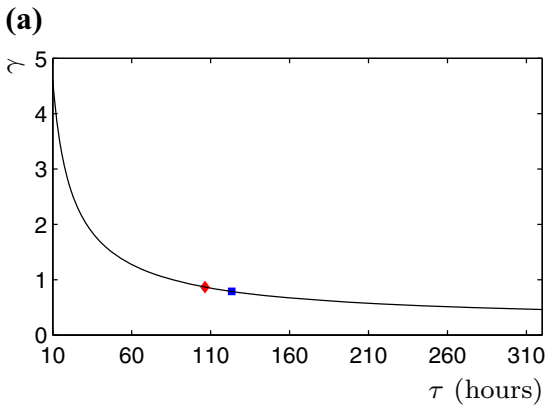

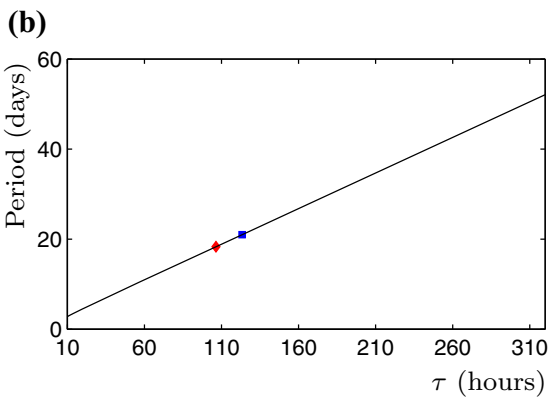

Fig. 5 Hopf bifurcation curve (τ, γ) and corresponding periods computed varying values of the transit rate a. The maturation time τ for each value of a was calculated as $\tau = n/a$, with $n = 4$. Red diamonds correspond to $\tau = 106.41$ h, its homeostasis value, with $\gamma = 0.86766$ and period of 18.32 days. Blue squares correspond to $\tau = 123.34$ h with $\gamma = 0.78911$ and period of 21.00 days. Remaining parameters are as in Table 1. **a** Hopf bifurcation curve for $\mathbf{X}_2^*$ in the (τ, γ) parameter space. **b** Period (in days) as a function of the maturation time τ for the Quartino model Eq. (2) (Color figure online)

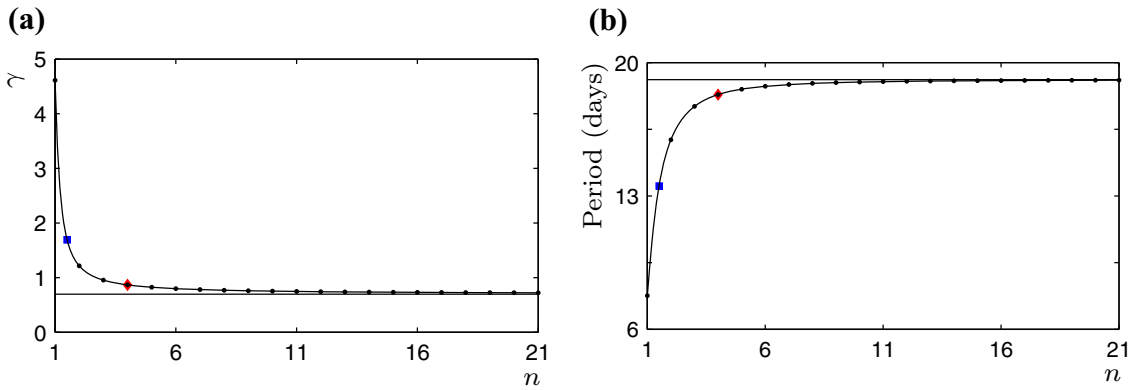

Fig. 6 Hopf bifurcation curve and corresponding periods. Value of γ and period of orbit at Hopf bifurcations as a and n are varied with $\tau = n/a$ kept constant. The black dots indicate integer values of n and correspond to bifurcations of $\mathbf{X}_2^*$ in the Quartino model, while the underlying smooth black curve applies to $\mathbf{Y}_2^*$ for the distributed DDE (Eq. 27) with integer or real n. Red diamonds correspond to $n = 4$, its homeostasis value, with $\gamma = 0.86766$ and period of 18.32 days. Blue squares correspond to $n = 1.5$ with $\gamma = 1.69292$ and period of 13.53 days. The horizontal lines correspond to the bifurcation point $\gamma = 0.69754$ and the corresponding period 19.11 days for the discrete DDE (Eq. 29). **a** Hopf bifurcation curve in (n, γ) parameter space. **b** Period (in days) as a function of n of bifurcating solution (Color figure online)

ourselves to changing τ, γ and n. Varying any of these parameters does not change the steady state $\mathbf{Y}_2^*$, and also leaves the corresponding elements of $\mathbf{X}_2^*$ unaltered. This then only changes the size of the transit compartments. Moreover, $G = G_0$ at these steady states, which implies that there is no time re-scaling and $\hat{t} = t$ at the steady state and its bifurcations.

Varying just γ, with the remaining parameters kept at their homeostasis values (see Table 1), we find that there is a Hopf bifurcation at $\gamma = 0.86766$, with the resulting periodic orbits having period 18.32 days at the bifurcation point. A limit cycle with a period characteristic of cyclic neutropenia [14] is found by varying both parameters. In Fig. 5, we show the Hopf bifurcation curve for $\mathbf{X}_2^*$ in the parameter space (τ, γ) for the Quartino model (Eq. 2); the steady state is stable in the region below the Hopf curve and unstable otherwise.

In the same vein, we also computed bifurcation points for the equilibrium $\mathbf{X}_2^*$ of distributed DDE model (Eq. (27)) using the characteristic Eq. (50) with $n = 4$. As expected, given that the this model is simply a trivial time-rescaling of the Quartino model (Eq. 2) we obtain the same bifurcation points shown in Fig. 5.

In the previous example as a is varied the mean delay $\tau = n/a$ also changes, so in Fig. 6 we illustrate the bifurcations as a, n and γ are all varied under the constraint that $\tau = n/a$ is kept constant at its homeostasis value. The Hopf bifurcation curve for the steady state $\mathbf{Y}_2^*$ of the distributed DDE model (Eq. 27) shown in Fig. 6 applies for all real $n > 0$ (with the blue squares illustrating the case of $n = 1.5$). The integer values of n also correspond to Hopf

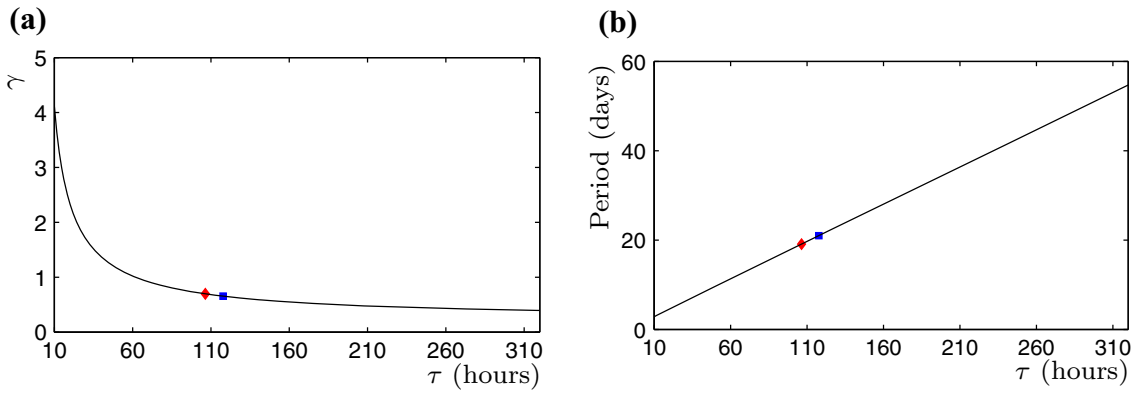

Fig. 7 Hopf bifurcation curve and corresponding periods for the discrete DDE of Eq. (27). Red diamonds correspond to τ at its homeostasis value of 106.41 h with $\gamma = 0.69754$ and a period 19.11 days. Blue squares correspond to $\tau = 117.75$ (h) with $\gamma = 0.65534$ and period 21.00 days. All other parameters are as in Table 1. **a** Hopf bifurcation curve for $\mathbf{Y}_2^*$ in the (τ, γ) parameter space. **b** Period (in days) as a function of τ for the discrete DDE model Eq. (29) (Color figure online)

Table 2 Hopf bifurcation points of the QSP model

Parameter (units)	Description	Homeostasis value	Hopf bifurcation	Period (days)
γ_Q (days^{-1})	HSC rate of apoptosis	0.1	0.22791	36.69
$\eta^h_{N_P}$ (days^{-1})	Proliferation rate at homeostasis	1.6647	7.4	60.31
$\eta^{min}_{N_P}$ (days^{-1})	Minimal rate of proliferation	1.4060	0.81	25.86
V_{max} (–)	Maximum maturation velocity	7.8669	93	5.20
b_V (ng/mL)	Maturation velocity half-effect concentration	0.24610	0.0184	5.20

For each line the Hopf bifurcation point was computed by changing the respective parameter and following the solution λ of Eq. (59) in the (σ, ω)-plane numerically, with the period given by $2\pi/\omega$. The parameters values at homeostasis were obtained from [13]

Table 3 Hopf bifurcations points of the QSP model

Parameters (units)	Hopf Bifurcation	Period (days)
(V_{max}, b_V) (–,ng/mL)	(30, 7.8)	5.20
(V_{max}, b_V) (–,ng/mL)	(61, 16.1)	5.20
$(b_{N_P}, \eta^{min}_{N_P})$ (ng/mL,days^{-1})	(0.065, 1.1)	25.86
$(\eta^h_{N_P}, \eta^{min}_{N_P})$ (days^{-1}, ng/mL)	(2, 1.1)	32.58

Hopf bifurcation points as in Table 2, but this time varying pairs of parameters with the other parameters at homeostasis values from [13]. V_{max}: Maximum maturation velocity; b_V: Maturation velocity half-effect concentration; b_{N_P}: Proliferation Michaelis-Menten constant; $\eta^{min}_{N_P}$: Minimal rate of proliferation; $\eta^h_{N_P}$: Proliferation rate at homeostasis

bifurcations of $\mathbf{X}^*_2$ of the Quartino model. The Hopf bifurcation for the discrete DDE (Eq. 27) is also illustrated and corresponds to the $n \to \infty$ limit of the bifurcation points for the Quartino model. The steady state is stable in the region below the Hopf curve and unstable otherwise.

Figure 7 shows the Hopf bifurcation curve for $\mathbf{Y}^*_2$ in the parameter space (τ, γ) for the discrete DDE model Eq. (29). The steady state is stable in the region below the Hopf curve and unstable otherwise. Blue squares represent a limit cycle with a period characteristic of cyclical neutropenia. The similarity between Figs. 5 and 7 underlines the equivalencies of the equivalent expressions of the Quartino model (Eq. 2) and the discrete DDE (Eq. 29), obtained by applying the linear chain technique.

Comparing the value of γ reflected by the red squares of Figs. 5, 6, and 7, we note that the region of stability for the discrete DDE model $\beta < \gamma < 0.69754$ is smaller than that of the distributed DDE with $n = 4$ (and of the equivalent ODE Quartino model), $\beta < \gamma < 0.86766$. Furthermore, in the limit $n \to \infty$ with $a = n/\tau$ or $a = (n+1)/\tau$, the characteristic roots of the distributed DDE model Eq. (50) converge to those of the discrete DDE model Eq. (47) when holding τ fixed, (see Fig. 6). This is expected since Eq. (50) approaches Eq. (47) when $n \to \infty$.

Bifurcations in the QSP model of granulopoiesis

We also studied whether parameter changes can lead the steady state $\mathbf{X}^*$ of QSP model (Eq. 30) to lose stability. We observed that changes in parameters related to proliferation and maturation lead to a loss of stability via a Hopf bifurcation, as reflected in Table 2. Additionally, we verified that the steady state remains stable when the half-maximal neutrophil proliferation constant b_{N_P}, the rate of maturing neutrophil death γ_{N_M}, or the rate of neutrophil apoptosis in the bone marrow reservoir γ_{N_R} is multiplied or divided by a factor of 100.

An additional Hopf bifurcation point leading to an orbit of period of 20.94 days was observed by changing four parameters simultaneously: $\eta^h_{N_P} = 1.7\,\text{days}^{-1}$; $b_{N_P} = 2.0$ ng/mL; $\eta^{min}_{N_P} = 1.3\,\text{days}^{-1}$; and $\tau_{N_P} = 6.1$ days. Table 3 reports the loss of stability via a Hopf bifurcation when pairs of parameters are varied in tandem.

It is worth noting that the granulopoietic system as reflected in the QSP model is very robust around homeostatic parameter values, and that physiologically realistic scenarios may even preclude reaching the bifurcation values. For example, in the case of $\eta^h_{N_P}$, the artificial removal of G-CSF from the body would be required to attain the bifurcation point.

Model selection and the impact of interindividual variability

When considering the time-rescaled Quartino model (Eq. 26) and discrete delay model (Eq. 29), the impact of interindividual variability (IIV) remains an open question. Since the discrete delay model is the equivalent of taking n to infinity in Eq. (26), we seek to quantify any altered behaviours due to IIV as n is increased. Here we must consider the PK/PD variability in both G-CSF and the chemotherapeutic drug thus, in what follows, E_{Drug} is no

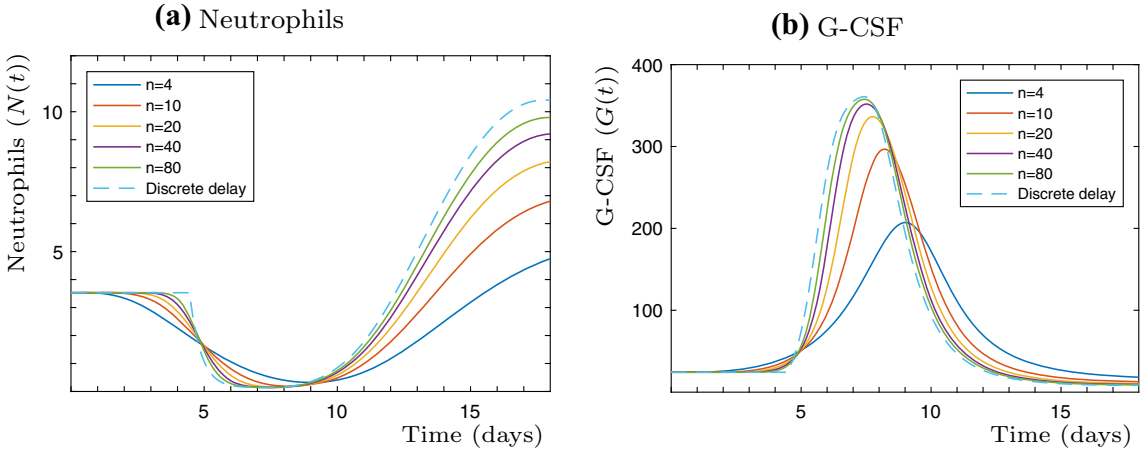

Fig. 8 Neutrophil and G-CSF concentrations from the generalised Quartino model of Eq. (2) and the equivalent time-rescaled discrete delay model Eq. (29) for increasing values of n. Since the discrete delay model in Eq. (29) is expressed in the time-rescaled $\hat{t}(t)$, we inverted Eq. (25) and mapped the simulated solution back to t to directly compare to Eq. (2). Dashed line: solution of discrete delay (Color figure online)

longer equal to 0. Instead, let C_{doc} be the concentration of docetaxel in the central compartment. As in [38], we consider a linear PD relationship between the concentration of docetaxel and its effect on the proliferation rates, so E_{Drug} = Slope $\times$ C_{doc}, where Slope is the linear drug effect. Using the docetaxel Pop-PK model of Bruno [6] and this linear effects model, 30 virtual patients were generated for both the generalised and time-rescaled Quartino models.

To ensure that we are comparing like models, τ was kept fixed as n was increased. In [38], the MMT for docetaxel was found to be 133 h. As alluded to in the caption of Table 1, we must apply a correction factor to account for the misspecification of the mean maturation time as $\text{MMT} = (n+1)/k_{tr}$ instead of $\text{MMT} = n\,/\,a$. Accordingly, we take $\tau = (4/5)\text{MMT} = (4/5) \times 133 = 106.4$, where the factor (4/5) accounts for the de-coupling the progenitor and maturing compartments. The initial conditions for both models are given by Eq. (7) ($N(0) = N_0$, and $G(0) = G_0$), and k_{tr} was taken to be equal to k_P, as in [38]. All other parameters are given as stated in Table 1.

We first verified that solutions to Eq. (2) were identical to the solutions to Eq. (26) when the latter were rescaled according to Eq. (25) (not shown). To visualise the impact of increasing n, we compared the predictions of Eqs. (2) to (29) (the case of n in the limit to infinity) using only the typical parameter estimates. As seen in Fig. 8, as $n \to \infty$, solutions to the generalised Quartino model (and equivalently, the time-rescaled Quartino and distributed delay models) converge to that of the discrete delay. As n increases, so too does the dimension of the resulting ODE system for Eq. (2), which is not the case for the 3 equations of Eq. (29).

We then compared the full Pop-PK predictions of Eq. (2) for these 30 virtual patients when $n = 4$ and $n = 10$. Keeping τ fixed while increasing n increases the variance $\sigma^2 = n/a^2$ of the gamma function in Eq. (11). We can observe this effect in Fig. 9, where including IIV and subsequently increasing n does not significantly affect the mean solution but does increase the spread of the distribution of solutions around the mean. Thus, for the chemotherapy-induced neutropenia models, there is a confounding relationship between interpatient variability in PK/PD parameters and the estimated number of artificial transit compartments.

Discussion

Mathematical pharmacology is increasingly recognised as a quantitative methodology critical to understanding pharmaceutical treatments and their efficacy while simultaneously raising compelling mathematical problems [45]. Using granulopoiesis as a backdrop, in the present paper we have examined the connections between the familiar PK/PD model formalism originally proposed by Friberg [20] and adapted by Quartino [38] and a discrete delay model of neutrophil production, connected via a distributed delay model. Crucially, we have shown how the stability of each model can be studied straightforwardly via this latter distributed delay model, underlining the advantage of being able to transfer between these equivalent expressions and motivating the present analysis. To that end, we demonstrated that solutions of the generalised (time-rescaled) Quartino transit compartment model converge to that of the time-rescaled discrete DDE model as $n \to \infty$. By examining the impact of the inclusion of IIV on the solutions to each of the models, we showed that variations related to increases to n cannot be explained separately from

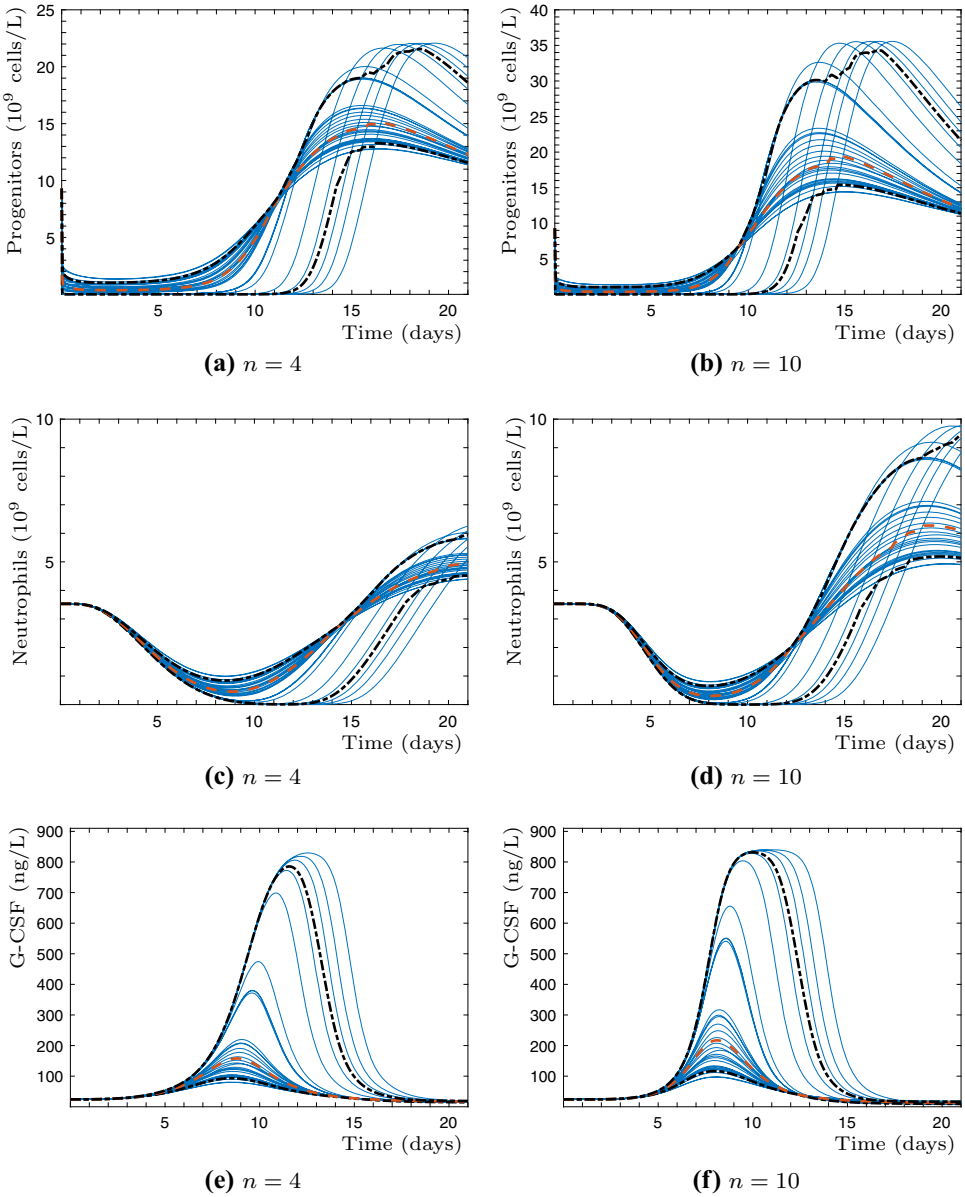

(a) $n = 4$ **(b)** $n = 10$ **(c)** $n = 4$ **(d)** $n = 10$ **(e)** $n = 4$ **(f)** $n = 10$

Fig. 9 Impact of IIV on the Quartino model Eq. (2) and its equivalent forms Eq. (26) and Eq. (27) for two different values of n. PopPK parameters for 30 virtual patients were generated following [6] and used as inputs to Eq. (2). Solid blue lines: individual predictions; black dotted-dashed lines: 10th and 90th percentiles of predictions; red dashed lines: median prediction (Color figure online)

presence of interindividual variability. Last, using our previously published QSP model of the negative feedback relationship between granulopoiesis and G-CSF, we have identified several Hopf bifurcations through bifurcation analysis, a technique not commonly applied in the classical PK/PD analyses, and reviewed the impact the interpretation of such bifurcations can have on our understanding of pharmacological systems when used in concert with more common sensitivity and variability analyses. We would like to highlight two results in particular. First, the distributed delay model Eq. (27) exhibits wider regions of stability around the steady state $\mathbf{Y}_2^*$ as compared to the discrete DDE model Eq. (29), consistent with the result that "distributed delays are inherently more stable than the same system with discrete delays" [7]. Second, we identified Hopf bifurcations in the distributed and discrete delay forms of the Quartino model with periods corresponding to those in cyclic neutropenic patients by varying the feedback parameter γ and the delay τ, demonstrating how bifurcation analyses can be applied in mathematical pharmacology to understand the pathogenesis towards diseases.

Perhaps the most immediately consequential conclusion drawn here is the incorrect definition of the mean transit/maturation time in the original and subsequent applications of the Friberg model. As previously mentioned, by setting $k_P = a = k_{tr}$ with $G(t) = G_0$, the MTT (sometimes MMT) was originally expressed as $(n+1)/k_{tr}$. However, we have shown that the mean delay of the distributed delay model is constant and instead given by $\tau = n/a$ (which,

when $a = k_{tr}$ is then clearly given by n/k_{tr}). Thus it is mathematically incorrect to set $\text{MMT} = (n+1)/k_{tr}$ as it treats the proliferative pool as an additional transit compartment and this formulation cannot be recovered via the linear chain technique. The generalised Quartino model Eq. (2) explicitly decouples the maturation time and the production rate of cells to eliminate this problem. Additionally, we highlighted the mathematical issue presented when the transit rates are non-constant, as in [38], to the derivation Eq. (14).

Further, since, in [20] and its various extensions and applications, the parameter k_{tr} is determined via the MMT, the mean maturation time is fit and then the rate of transit through each compartment is determined via the equation $\text{MMT} = (n+1)/k_{tr}$. Mathematically, this introduces additional difficulties since, in general, $\tau = n/a$, where a is not necessarily equal to k_{tr} nor k_P. Crucially, however, setting $\text{MMT} = (n+1)/k_{tr}$ leads to disparate estimates for the maturation process, ranging, for example, from 102 h ($n = 6$) in [37] to 210 h ($n = 4$) in [38]. Although there will be a wide range of MMTs during pathological conditions and/or during treatment with exogenous cytokines, the physiology of these changes are due to the cytokine paradigm and the speeding up of the maturation process by G-CSF [35]. In contrast, labelling studies report a much narrower range of maturation times (153.6 h in [35] and 165.6 h in [15], for example) during homeostatic conditions. Thus, differences in reported MMT arise not from a wide range of mean maturing times across individuals but are due instead to transient effects brought on by increased (or decreased) G-CSF concentrations. Allowing the MMT to vary widely in the context of chemotherapeutic treatment is therefore better explained by fixing a value from homeostatic studies and explicitly modelling the effects of G-CSF.

We therefore emphasise that this work provides further motivation to systematically incorporate, from first principles, the physiological architecture yielding the proper mathematical formulation of pharmacological models.

Acknowledgements DCS was supported by National Council for Scientific and Technological Development of Brazil (CNPq) postdoctoral fellowship 201105/2014-4. MC was supported by an Natural Sciences and Engineering Research Council of Canada (NSERC) postdoctoral fellowship and Grant DP5OD019851 from the Office of the Director at the National Institutes of Health to her PI. TC was supported by the Alberta government via the Sir James Lougheed Award of Distinction as well as the Centre de recherches mathématiques, Montréal. FN and JL are funded by FN's NSERC Industrial Chair in Pharmacometrics, supported by Novartis, Pfizer, and inVentiv Health Clinics, and an FrQNT projet d'équipe. JB and ARH are grateful to NSERC, Canada for funding through the Discovery Grant program. We are appreciative for our many very useful discussions with Michael C. Mackey.

References

1. Adimy M, Crauste F (2007) Modelling and asymptotic stability of a growth factor-dependent stem cells dynamics model with distributed delay. Discret Contin Dyn Syst Ser B 8(1):19–38
2. Agoram B, Woltosz W, Bolger M (2001) Predicting the impact of physiological and biochemical processes on oral drug bioavailability. Adv Drug Deliv Rev 50:S41–S67
3. Bélair J, Rimbu A (2015) Time delays in drug administration: effect, transit, tricks and oscillations. IFAC PapersOnLine 48(12):111–116
4. Beretta E, Breda D (2016) Discrete or distributed delay? effects on stability of population growth. Math Biosci Eng 13(1):19–41
5. Brooks G, Langlois G, Lei J, Mackey M (2012) Neutrophil dynamics after chemotherapy and G-CSF: the role of pharmacokinetics in shaping the response. J Theor Biol 315:97–109
6. Bruno R, Vivier N, Vergniol J, De Phillips S, Montay G, Sheiner L (1996) A population pharmacokinetic model for docetaxel (taxotere®): model building and validation. J Pharmacokinet Biopharm 24:153–172
7. Campbell S, Jessop R (2009) Approximating the stability region for a differential equation with a distributed delay. Math Models Nat Phenom 4(2):1–27
8. Christopher M, Link D (2007) Regulation of neutrophil homeostasis. Curr Opin Hematol 14:3–8
9. Colijn C, Mackey M (2005) A mathematical model of hematopoiesis: II. Cyclical neutropenia. J Theor Biol 237:133–146
10. Cooke K, Grossman Z (1982) Discrete delay, distributed delay and stability switches. J Math Anal Appl 86:592–627
11. Cooke K, Hang W (1996) On the problem of linearization for state-dependent delay differential equations. Proc AMS 124(5):1417–1426
12. Craig M (2017) Towards quantitative systems pharmacology models of chemotherapy-induced neutropenia. CPT Pharmacomet Syst Pharmacol 6(5):293–304
13. Craig M, Humphries A, Mackey M (2016) A mathematical model of granulopoiesis incorporating the negative feedback dynamics and kinetics of G-CSF/neutrophil binding and internalisation. Bull Math Biol 78(12):2304–2357
14. Dale D, Mackey M (2015) Understanding, treating and avoiding hematological disease: better medicine through mathematics? Bull Math Biol 77:739–757
15. Dancey J, Deubelbeiss K, Harker L, Finch C (1976) Neutrophil kinetics in man. J Clin Investig 58:705–715
16. Dixit N, Perelson A (2004) Complex patterns of viral load decay under antiretroviral therapy: influence of pharmacokinetics and intracellular delay. J Theor Biol 226:95–109
17. Foley C, Mackey M (2008) Mathematical model for G-CSF administration after chemotherapy. J Theor Biol 257:27–44
18. Foley C, Mackey M (2009) Dynamic hematological disease: a review. J Math Biol 58:285–322
19. Friberg L, Karlsson M (2003) Mechanistic models for myelosuppression. Investig New Drugs 21:183–194
20. Friberg L, Henningsson A, Maas H, Nguyen L, Karlsson M (2002) Model of chemotherapy-induced myelosuppression with parameter consistency across drugs. J Clin Oncol 20:4713–4721
21. Goudriaan J, Gurney WSC, Nisbet RM, Blythe SP (1986) Numerical approaches. In: Metz JAJ, Diekmann O (eds) The dynamics of physiologically structured populations. Springer, Berlin, pp 452–494
22. Gruber M, Fleiss K, Porpaczy E et al (2011) Prolonged progression-free survival in patients with chronic lymphocytic leukemia receiving granulocyte colony-stimulating factor during treatment with fludarabine, cyclophosphamide, and rituximab. Ann Hematol 90:1131–1136

23. Hearn T, Haurie C, Mackey M (1998) Cyclical neutropenia and the peripherial control of white blood cell production. J Theor Biol 192:167–181
24. Jacquez JA, Simon CP (2002) Qualitative theory of compartmental systems with lags. Math Biosci 180(1–2):329–362
25. Jamei M, Turner D, Yang J, Neuhoff S, Polak S, Rostami-Hodjegan A, Tucker G (2009) Population-based mechanistic prediction of oral drug absorption. AAPS J 11(2):225–237
26. Krinner A, Roeder I, Loeffler M, Scholz M (2013) Merging concepts—coupling an agent-based model of hematopoietic stem cells with an ODE model of granulopoiesis. BMC Syst Biol 7:117
27. Krzyzanski W (2011) Interpretation of transit compartments pharmacodynamic models as lifespan based indirect response models. J Pharmacokinet Pharmacodyn 38:179–204
28. Lyman G, Dale D (2011) Introduction to the hematopoietic growth factors. In: Lyman GH, Dale DC (eds) Hematopoietic growth factors in oncology. Springer, Berlin
29. MacDonald N (1978) Time lags in biological models. Springer, Berlin
30. MacDonald N (1989) Biological delay systems: linear stability theory. Cambridge University Press, Cambridge
31. Mackey M, Milton J (1990) Feedback, delays, and the origin of blood cell dynamics. Comments Theor Biol 1:299–327
32. Mantovani A, Cassatella MA, Costantini C, Jaillon S (2011) Neutrophils in the activation and regulation of innate and adaptive immunity. Nat Rev Immunol 11:519–531
33. Mathworks (2013) MATLAB 2016b. Mathworks, Natick, Massachusetts
34. Meiss J (2007) Differential dynamical systems. Society for Industrial and Applied Mathematics, Philadelphia, PA
35. Price T, Chatta G, Dale D (1996) Effect of recombinant granulocyte colony-stimulating factor on neutrophil kinetics in normal young and elderly humans. Blood 88:335–340
36. Pujo-Menjouet L (2016) Blood cell dynamics: half of a century of modelling. Math Model Nat Phenom 11(1):92–115
37. Quartino A, Friberg L, Karlsson M (2012) A simultaneous analysis of the time-course of leukocytes and neutrophils following docetaxel administration using a semi-mechanisitic myelosuppression model. Investig New Drugs 30:833–845
38. Quartino A, Karlsson M, Lindman H, Friberg L (2014) Characterization of endogenous G-CSF and the inverse correlation to chemotherapy-induced neutropenia in patients with breast cancer using population modeling. Pharm Res 31(12):3390–3403
39. Rankin S (2010) The bone marrow: a site of neutrophil clearance. J Leukoc Biol 88:241–251
40. Schirm S, Engel C, Loeffler M, Scholz M (2014) Modelling chemotherapy effects on granulopoiesis. BMC Syst Biol 8:138
41. Smith H (2011) An introduction to delay differential equations with applications to the life sciences. Springer, New York
42. Steimer JL, Plusquellec Y, Guillaume A, Boivieux JF (1982) A time-lag model for pharmacokinetics of drugs subject to enterohepatic circulation. J Pharm Sci 71(3):297–302
43. Sternberg C, de Mulder P et al (2006) Seven year update of an EORTC phase III trial of high-dose intensity M-VAC and G-CSF versus classic M-VAC in advanced urothelial tract tumours. Eur J Cancer 42:50–54
44. Vainstein V, Ginosar Y, Shoham M, Ranmar D, Ianovski A, Agur Z (2005) The complex effect of granulocyte colony-stimulating factor on human granulopoiesis analyzed by a new physiologically-based mathematical model. J Theor Biol 235:311–327
45. van der Graaf PH, Benson N, Peletier LA (2016) Topics in mathematical pharmacology. J Dyn Differ Equ 28(3):1337–1356
46. Vogel T (1963) Systèmes déferlants, systèmes héréditaires, systèmes dynamiques. In: Proceedings of the international symposium nonlinear vibrations, IUTAM, Kiev, 1961, Academy of Sciences USSR, pp 123–130
47. Vogel T (1965) Théorie des Systèmes Evolutifs. Gautier Villars, Paris
48. von Vietinghoff S, Ley K (2008) Homeostatic regulation of blood neutrophil counts. J Immunol 181:5183–5188
49. Ward AC, Aesch YMV, Gits J, Schelen AM, Koning JPD, Leeuwen DV, Freedman MH, Touw IP (1999) Novel point mutation in the extracellular domain of the granulocy colony-stimulating factore (G-CSF) receptor in a case of severe congenital neutropenia hyporesponsive to G-CSF treatment. J Exp Med 190(4):497–507